A REVIEW ON DOCKING STUDIES OF INDOLE MOIETY AS POTENT INHIBITOR OF TUBULIN POLYMERIZATION

Aditya Dixit[a]*, Devender Pathak[b] and Gyanendra Kumar Sharma[a]

Keywords: Vincristine; docking; Colchicine; Tubulin.

Aromatic heterocycles especially indole plays an important part in treatment of cancer. This review highlights compounds in development bearing indole moiety in their scaffold for the treatment of cancers. This review also highlights the utilization of colchicine binding site in order to inhibit tubulin polymerization. Docking studies shows that colchicine binding site is used by various indole derivatives to exert their action. Vincristine and vinblastine are the natural compounds which have the anticancer activity but they act on the vinca domain of the tubulin protein. Vinca domain can be too large for small ligands, so small molecules can utilize colchicines binding site to inhibit microtubule polymerization.

* Corresponding Authors
Phone: +919258474535
E-Mail: adixit70@gmail.com
[a] Rajiv Academy for Pharmacy, Mathura, U.P., India
[b] Pharmacy College, Saifai, Etawah, U.P., India

Introduction

The design and discovery of more effective and safer anticancer drug candidates are of interest in contemporary medicinal chemistry. Despite continued research efforts, cancer remains as a death cause of a large population of the world. There is enough scope to develop new compounds which can possess good antiproliferative action with different site of binding. When we talk about the anticancer agents, microtubules can be a good target in order to achieve cell cycle arrest. Microtubules are important in mitosis and have been recognized as an important target for the development of novel anticancer drugs. Microtubule formation involves polymerization as well as depolymerization of α and β tubulin dimers. Regulation of this process is strictly done by different regulatory proteins after expressing various tubulin forms (6 types of α-tubulin and 7 types of β-tubulin).[1] Therefore if tubulin is targeted, it would have been important route to anticancer therapy. A vast number of natural products like Paclitaxel, Vincristine, Combretastatin A-4 and Colchicines are there which can induce cell apoptosis through interference with polymerization and depolymerization of tubulin. Colchicine is a naturally occurring antimitotic agent, it resembles cis-stilbene and acts at same binding site of microtubule.[2,3,4] The microtubules have three ligand binding sites-vinca domain,[5] colchicine domain[6] and taxol domain.[7]

Indole as Tubulin Polymerization Inhibitor

Sunil et al reported the synthesis of three types of indole derivatives, 3-(1-benzyl-1*H*-indol-2-yl)-2*H*-chromen -2-ones,[8] 2-(2-oxo-2H-chromen-3-yl)-1*H*-indol-3-carbaldehydes[9] and 2-(2-oxo-2*H*-chromen-3-yl)-1*H*-indol-3-carboxylicacid.[10] Docking studies (Figure 1) were performed on BCl-2 (B-Cell lymphoma-2) which is an apoptosis related gene. Cytotoxic effect in a dose dependent manner was observed when tested on human breast adenocarcinoma (MCF-7).[11] Vincristine was taken as a standard drug. Compound (**1**) was found to be most potent.[12]

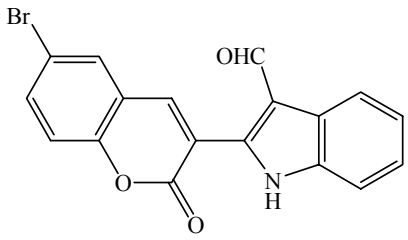

(**1**)

Docking studies of novel arylthioindoles (ATIs) with tubulin protein have been reported. All studies were performed on a MacPro dual 2.66 GHz Xeon by Ubuntu 9. The tubulin structure was downloaded from PDB data bank (http://www.rcsb.org)-PDBID:1SAO,[13] 3KHC and 3KHE.[14] Compound (**2**) was found to be the most potent candidate.[15]

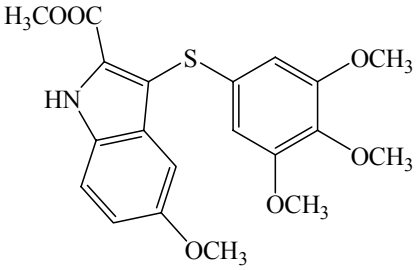

(**2**)

1-(4'-Indolyl and 6'-quinolyl)indoles were synthesized and evaluated for biological activity by Lai et al.[16] Docking was performed on colchicine binding site with Gold 4.0 software to evaluate inhibition of microtubule polymerization. Compounds (**3**) and (**4**) (Figure 3) were found to be most potent among the synthesized derivatives.[16]

Huang et al established the SARs of 2,4-disubstituted furo [3,2-*b*] indole derivatives. They synthesized the compounds and anticancer activity was evaluated against NCI-60 (National Cancer Institute-60) and A498 renal cancer cell lines.[17,18] Compound (**5**) (figure 4) was found to be most potent.[19]

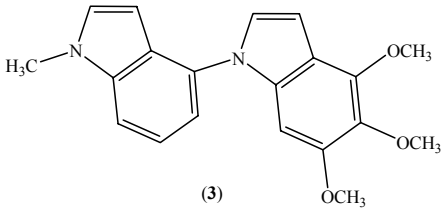

(**3**)

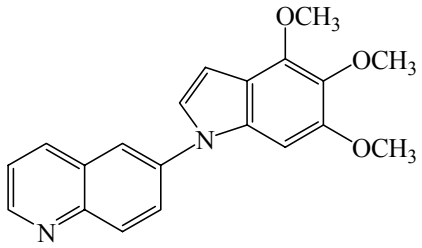

(**4**)

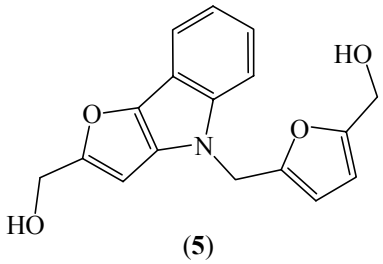

(**5**)

Design and synthesis of some pyrazole-oxindole conjugates has been reported for targeting tubulin polymerization. Twenty-one compounds were synthesized through Knoevenagel condensation reaction and their activity against different cancer cell lines was investigating.[20,21,22] Docking studies were performed on three lead compounds. They were docked against tubulin structure (PDB code: 3E22) and they showed the disruption of microtubule network via colchicine binding site.[23,24,25] Compounds (**6**) and (**7**) were found to be most potent.[26]

Pyrano-chalcone derivatives containing indole moiety have been designed, synthesized and evaluated for ant-tubulin activity. A molecular docking study was performed by Genetic Optimization of Ligand Docking (GOLD). They induced cell cycle arrest in G2/M phase and inhibited tubulin polymerization in colchicine binding site and anticancer activity was exerted against HepG2 human liver carcinoma.[27] Compound (**8**) was having the best activity amongst all the derivatives.[28]

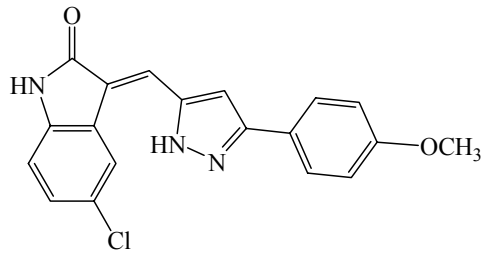

(**6**)

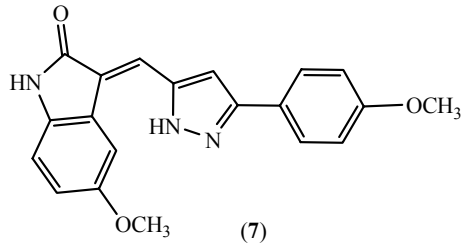

(**7**)

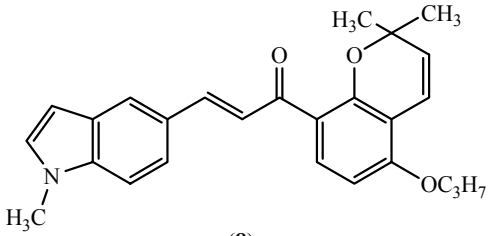

(**8**)

Synthesis of trans-indole-3-acrylamide derivatives and their activity was investigated against proliferation of human cancer cell lines (HeLa, MCF-7, MDA-MB-231, Raji and HL-60) by MTT assay. Compound (**9**) was found to be most active against both Raji and HL-60 cell lines. IC_{50} values were 9.5 & 5.1 μM. Docking studies were performed with tubulin/DAMA colchicine complex (PDB ID: 1SA0).[13,29]

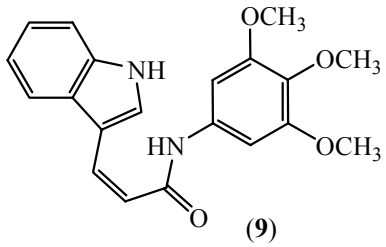

(**9**)

Docking and synthesis of indole and carbazole analogues has been done. It has been mentioned that the tubulin has three sites, taxane, vincamycin and colchicines sites. Vincamycin and taxane are complex molecules whereas colchicine is less complex so it attracts the scientists.[30-34] High content Cellular Analysis (HCA) of compound (**10**) (carbazole urea analogue) with cells shown that it causes cell apoptosis by blocking G2/M progression and shows similar effects as that of Paclitaxel and Vinblastine.[35] Compound (**11**) was found to be most potent among indole derivatives.[36]

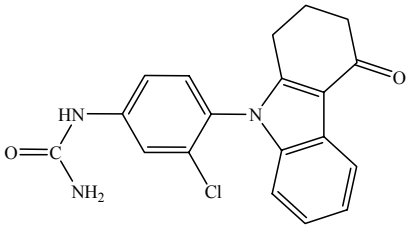

(**10**)

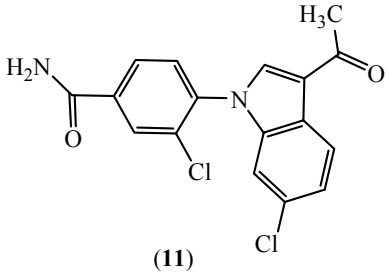

(**11**)

About 160 indole derivatives have been synthesized. 2-Aroylindoles were found orally active tubulin inhibitors. Tubulin binding assay was carried out according to Tahit et al.[37] Tubulin GTP assay was carried out according to the modifications done by Roychowdhury et al.[38] Compound (**12**) was found to be most potent against all tested cell lines.[39]

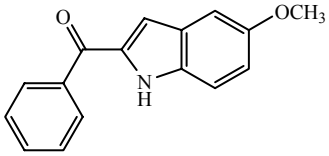

(**12**)

Antimitotic and antitumor activity of novel indole compounds has been reported. Many 3-aroylindoles have been designed and synthesized as combretastatin A-4 (CA-4) analogs for evaluation of biological activity.[40] In-vitro assay of microtubule assembly was performed according to the procedure discussed by Bollag et al.[41] In vivo assay of microtubule assembly was performed according to the Blagosklommy et al.[42] Among all derivatives, 6-methoxy-3-(3',4',5'-trimethoxy-benzoyl)-1*H*-indole (**13**) was found to be best lead compound in a concentration dependent manner.[43]

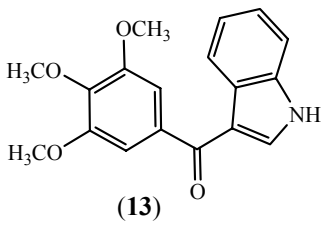

(**13**)

Synthesis and molecular docking of indole-pyrimidine derivatives have been described. The inhibition of tubulin polymerization has been related with colchicine binding site. For *in-vitro* tubulin polymerization assay, tubulin was taken from pig brain which was isolated by the method given by Shelanski et al.[44]The molecular modeling studies were performed with surflex-dock module and the tubulin protein structure was downloaded from protein data bank (PDB). Energy minimization of molecules was done by using tripos force field.[45] It was found that compound (**14**) was having best binding characteristics with colchicine binding site[46] and it occupies the same pocket as that of CA 224.[47]

Synthesis and biological activity of stable inhibitors of colchicine binding site of tubulin heterodimer have been reported. The importance of TMP (3,4,5,-trimethoxyphenyl) moiety for the growth inhibition of tumor cells have been ascertained.[48,49,50] It was found that 4-substituted methoxybenzoyl-aryl-thiazole (SMART)[51], 2-aryl-4-benzoyl-imidazole (ABI)[52], and phenylaminothiazole (PAT)[53] are good anticancer agents. These agents are active even at the nanomolar concentrations on many cell lines but their pharmacokinetics showed that their bioavailability is poor. It was due to the two major metabolic reactions in the microsomes of the liver i.e. carbonyl reduction and demethylation of TMP ring.[54] Three sets of new analogs were synthesized by the modifications at carbonyl linker of preexisting potent compounds, which were originally having short half life (17 minutes) or which were metabolically labile. Compounds (**15**) and (**16**) were found to be most potent with enhanced half life.[55]

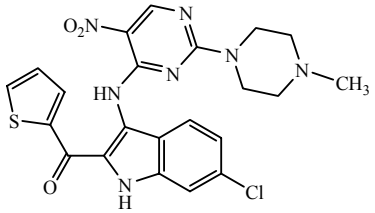

(**14**)

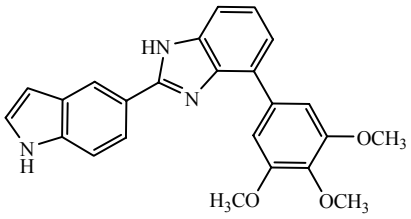

(**15**)

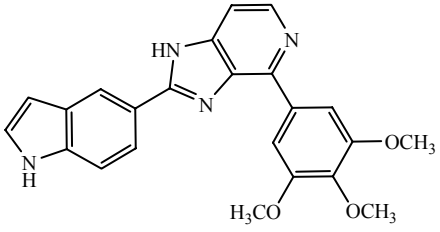

(**16**)

Mechanism of qction

All the papers show that the compounds inhibited the tubulin polymerization after binding with the colchicine domain of the tubulin. Taxanes act by stabilizing the microtubule whereas vinca and colchicines act by destabilizing the microtubules. The inhibition of tubulin polymerization results in the cell cycle arrest in G2/M phase and causes apoptosis.

Conclusion

It has been shown in this review that indole moiety is present in structure of various antimitotic agents. Colchicine binding site itself captured the interest of the researchers in recent time. Complexity of vinca and taxane domain resulted in the enhancement of the optimization of colchicines binding analogues. Advantages due to which colchicines binding site got attention are high potency, relatively simple compounds for optimization, toxicity is selective for tumor vasculature and their ability to withstand with the P-glycoprotein efflux pump mediated multidrug resistance. It also shows that the colchicine binding site is the preferred site for the binding for indole derivatives to exert anticancer activity.

References

[1]Jordan, A. M., Wilson, L., *Nature Rev.***2004**, *4*, 253-265.

[2]Cushman, M., Nagarathnam, D., He, H. M., Lin, C. M., Hamel, E., *Eur. J. Med. Chem.,***1992**, *35*, 2293-3306.

[3]Nguyen, T. L., McGrath, C., Hermone,A. R., Burnett, D. W., Zaharevitz, B. W., Day, B. W., Wipf,P., Hamel, E., Gussio, R. A., *J. Med. Chem.,***2005**, *48*, 6107-6116.

[4]Ducki, S., Mackenzie, G., Greedy, B., Armitage, S., Chabert, J. F. D., Bennett, E., Nettles, J., Snyder, J. P, Lawrence, N. J., *Bioorg.Med. Chem*. **2009**, *17*, 7711-1722.

[5]Rai, S. S., Wolff, J., *J.Biol. Chem.,***1996**, *271*, 14707-14711.

[6]Haar, E., Rosenkranz, H. S., Hamel, E., Day, B. W., *Bioorg. Med. Chem.*, **1996**, *4*, 1659-1671.

[7]Andreu, J. M., Barasoain,I., *Biochem.,* **2001**, *40*, 11975-11984.

[8]Billimoria, A. D., Cava, M. P., *A. J. Org. Chem.*, **1994**, *59(22)*, 6777-6782.

[9]Jha, M., Edmunds, M., Lund, K., Ryan, A., *Tetrahedron Lett*. **2014**, *55*, 5691-5694.

[10]Zahran, M. A. H., Ibrahim, A. M. *J. Chem. Sci.,* **2009**, *121*, 455-462.

[11]Dixit, A., Pathak, D., Sharma, G. K., *Asian J. Pharm. Res. Dev.,* **2014**, *2*, 141-145.

[12]Sunil, D., Kamath, P. R., Ajees, A. A., Pai, K. S. R., Das, S., *Biorg. Med. Chem*., **2015**, *63*, 101-109.

[13]Ravelli, R. B., Gigant, B., Curmi, P. A., Jourdain, I., Lachkar, S., Sobel, A., Knossow, M., *Nature,* **2004**, *428*, 198-202.

[14]Dorleans, A., Gigant, B., Ravelli, R. B., Mailliet, P., Mikol, V., Knossow, M., *PNAS, USA*, 2009, *106*, 13775-13779.

[15]Coluccia, A., Sabbadin, D.,Brancale, A., *Eur. J. Med. Chem.,* 2011, *46*, 3519-3525.

[16]Lai, M. J., Chang, J. Y., Lee, H. Y., Kuo, C. C., Lin, M. H., Hsieh, H. P., Chang, C. Y., Wu, J. S., Wu, S. Y., Shey, K. S. ,Liou, J. P., *Eur. J. Med. Chem.***2011**, *46*, 3623-3629.

[17]Monks, A., Scudiero, D., Skehan, P., Shoemaker, R., Paull, K.,Visitica, D., Hose, C., Langley, J., Cronise, P., Vaigro-Wolf, A., Gray-Goodrich, M., Campbell, H., Mayo, J., Boyd, M. J., *Natl. Cancer Inst.*, **1991**, *83*, 757-766.

[18]Chen, C. J.,Hsu, M. H.,Huang, L. J.,Yamori, T.,Chung, J. G.,Lee, F. Y.,Teng, C. M.,Kuo, S. C., *Biochem. Pharmacol.,***2008** 75, 360-368.

[19]Huang, L. J., Zhuang, S .H., Lin, H. Y., Huang, C. H., Lien, J. C., Kuo, S. C., *Eur. J. Med. Chem.,***2013**, *66*, 466-479.

[20]Caballero, J., Munoz, C., Alzate-Morales, J. H., Cunha, S., Gano, L., Bergmann, R., Steinbach, J., Kneiss, T., *Eur. J. Med. Chem.*, **2012**, *58*, 272-280.

[21]Singh, P., Kaur, M., Holzer, W., *Eur. J. Med. Chem.,* **2010**, *4*, 4968-4982.

[22]Zhong, Y., Xue, M., Zhao, X., Yuan, J., Liu, X., Huang, J., Zhao, Z., Li, H., Xu, Y., *Bioorg. Med. Chem.,* **2013**, *21*, 1724-1734.

[23]Auto Dock, version 4.0, http://www.scripps.edu /mb/olson/doc/autodock/.

[24]Morris, G. M., Goodsell, D. S., Hallidav, R. S., Huey, R., Hart, W. E., Belew, R. K., Olson, A. J., *J.Comput. Chem.***1998**, *19*, 1639-1662.

[25]DeLano, W. L., DeLano Scientific, San Carlos, CA, USA, http://www.pymol.org.

[26]Kamal, A., Shaik, A. B., Jain, N., Kishor, C., Nagabhushana, A., Supriya, B., Kumar, G. B., Chaurasiya, S. S., Suresh, Y., Mishra, R. K., Addlagatta, A., *Eur. J. Med. Chem.*, **2015**, *92*, 501-13.

[27]Sherer, C., Snape, T. J., *Eur. J. Med. Chem.,* **2015**, *97*, 552-560.

[28]Wang, G. C., Li, C., He, L., Lei, K., Wang, F., Pu, Y., Yang, Z., Cao, D., Ma, L., Chen, J., Sang, Y., Liang, X., Xiang, M., Peng, A., Wei, Y., Chen, L., *Bioorg. Med. Chem.,* **2014**, *22*, 2060-2079.

[29]Baytas, S. N., Inceler, N., Yilmaz, A., Olgac, A., Meneuse, S., Benoglu, E., Hamel, E., Bortolozzi, R., Viola, G., *Bioorg. Med. Chem.,* **2014**, *22*, 3096.

[30]Nguyen, T. L., McGrath, C., Hermone, A. R., Brunette, J. C., Zaharevitz, D. W., Day, B. W., Wipf, P., Hamel, E., Gussio, R., *J. Med. Chem.,* **2005**, *48*, 6107-6116.

[31]Pelletier, P. S., Caventon, A., *J. Ann. Chim. Phys*., **1820**, *14*, 69.

[32]Pettit, G. R., Singh, S. B., Boyd, M. R., Hamel, E., Pettit, R. K., Schmidt, J. M., Hogan, F., *J. Med. Chem.,* **1995**, *38*, 1666.

[33]Koyanagi, N., Nagasu, T., Fujita, F., Watanabe, T., Tsukahara, K., Funahashi, Y., Fujita, M., Taguchi, T., Yoshino, H., Kitoh, K., *Cancer Res.*, **1994**, *54(7)*, 1702-6**.**

[34]De Brabander, M. J., Van de Veire, R. M., Aerts, F. E., Borgers, M., Janssen, P. A., *Cancer Res.,* **1976**, *36(3)*, 905-16.

[35]Barabasz, A., Foley, B., Otto, J. C., Scott, A., Rice, J., *Assay Drug Dev. Technol.,***2006**, 4,153.

[36]Barta, T. E., Barabasz, A. F., Briana, E. F., Geng, L., Hall, S. E., Hanson, G. J., Jenks, M., Ma, W., Rice, J. W., Veal, J., *Bioorg. Med. Chem. Lett.,***2009**, 19,3078.

[37]Tahir, S. K., Kovar, P., Rosenberg, S. H., Ng, S. C., *Biotechniques.,* **2000**, *29(1)*, 156-60.

[38]Roychowdhury, S., Panda, D., Wilson, L., Rasenick, M. M., *J. Biol. Chem.,* **1999**, *7(19)*, 13485-90.

[39]Beckers, T., Reissmann, T., Schmidt, M., Burger, A., Fiebig, H. H., Vanhoefer, U., Pongratz, H., Hufsky, H., Hockemeyer, J., Frieser, M., Mahboobi, S., *Cancer Res.,***2002**, *62*, 3113-3119.

[40]Nam, N. H., *Curr. Med. Chem.,* **2003**, *10(17)*, 1697-722.

[41]Bollag, D. M., McQueney, P. A., Zhu, J., Hensens, O., Koupal, L., Liesch, J., Goetz, M., Lazarides, E., Woods, C. M., *Cancer Res.,* **1995**, *55(11)*, 2325-33.

[42]Blagosklonny, M. V., Schulte, T. W., Nguyen, P., Mimnaugh, E. G., Trepel, J., Neckers, L., *Cancer Res.,* **1995**, *55(20)*, 4623-6.

[43]Kuo, C. C., Hsieh, H. P., Pan, W. Y., Chen, C. P., Liou, J. P., Lee, S. J., Chang, Y. L., Chen, L. T., Chen, C. T, Chang, J. Y., *Cancer Res.,* **2004**, *64(13)***,** 4621-28.

[44]Michael, L., Shelanski, F. G., Charles, R., *Proc. Natl. Acad. Sci. U S A.,* **1973**, *70(3)*, 765–768.

[45]Clark, M., Cramer, R. D., *J. Comput. Chem.,***1989**, *10*, 982.

[46]Mahale, S., Bharate, S. B., Manda, S., Joshi, P., Bharate, S. S., Jenkins, P. R., Vishwakarma, R. A., Chaudhuri, B., *J. Med. Chem.*, **2014**, *57*, 9658-9672.

[47]Hu, M. J., Zhang, B., Yang, H. K., Liu, Y., Chen, Y. R., Ma, T. Z., Lu, L., You, W. W., Zhao, P. L., *Chem. Biol. Drug. Des.,* **2015**, *86(6),*1491-500. doi: 10.1111/cbdd.12616.

[48]Álvarez, C., Álvarez, R., Corchete, P., Pérez-Melero, C., Peláez, R., Medarde, M., *Eur. J.Med. Chem.,* **2010***,* 45(2), 588-597.

[49]Brancale, A., Silvestri, R., *Med. Res. Rev.,* **2007**, *27(2)*, 209-38.

[50]Ray,K., Bhattacharyya, B., Biswas, B. B., *J. Biol. Chem.,* **1981**, *256(12)*, 6241-4.

[51]Lu, Y., Li, C. M., Wang, Z., Ross, C. R., Chen, J., Dalton, J. T., Li, W., Miller, D. D., *J. Med. Chem.,* **2009**, *52 (6)*, 1701-1711.

[52]Chen, J., Li, C. M., Wang, J., Ahn, S., Wang, Z., Lu, Y., Dalton, J. T., Miller, D. D., Li, W., *Bioorg .Med. Chem.,* **2011**, *19(16)*, 4782-95. doi: 10.1016/j.bmc.2011.06.084.

[53]Li, C. M., Chen, J., Lu, Y., Narayanan, R., Parke, D. N., Li, W., Ahn, S., Miller, D. D, Dalton, J. T., *Drug. Metab. Dispos.,* **2011**, *39(10)*, 1833-9. doi: 10.1124/dmd.110.036616.

[54]Li, C. M., Wang, Z., Lu, Y., Ahn, S., Narayanan, R., Kearbey, J. D., Parke, D. N., Li,W., *Cancer Res.,* **2011**, *71 (1)*, 216-224.

[55]Lu, Y., Chen, J., Wang, J., Li, C. M., Ahn, S., Barrett, C. M., Dalton, J. T., Li, W., Miller, D. D., *J. Med. Chem.,* **2014**, *57(17),* 7355-66. doi: 10.1021/jm500764v.

Received: 13.12.2016.
Accepted: 05.01.2017.

SYNTHESIS AND CHARACTERIZATION OF METAL COMPLEXES OF SCHIFF BASE LIGANDS DERIVED FROM 4-AMINOANTIPYRINE WITH 4-AMINOBENZOIC ACID AND BENZOIN

Rehab K. Al-Shemary[a]* and Maysoon T. Tawfiq[a]

Keywords: Benzoin; 4-aminobenzoic acid; 4-aminoantipyrine; Schiff bases, metal complexes; biological activity.

Two chelate-forming Schiff bases derived from 4-aminoantipyrine with 4-aminobenzoic acid and benzoin, namely (Z)-4-(4-amino-1,5-dimethyl-2-phenyl-1H-pyrazol-3(2H)-ylideneamino)benzoic acid (HL^1) and 4-((E)-4-((E)-((R)-2-hydroxy-1,2-diphenylethylidene)amino)-1,5-dimethyl-2-phenyl-1H-pyrazol-3(2H)-ylideneamino)benzoic acid (H_2L^2) were prepared and complexed with copper(II), nickel(II), cobalt(II), manganese(II) and mercury(II)chlorides in ethanol. The $M(HL^1)_2Cl_2$ and $M(HL^2)_2$ type complexes could be isolated. The ligands and theirs metal complexes were characterized using elemental analysis, infrared and electronic, ^1H and ^{13}C NMR spectroscopy, molar conductance and magnetic moment measurements. The measurements showed that the HL^1 ligand is coordinated in their complexes with N,N-bidendate mode, while HL^2 ionic ligand in NNO tridentate pattern through the azomethine nitrogen, amino-group and the depotonated hydroxyl group of benzoin. The stability constants of complexes were determined spectrophotometricaly. All the studies reveal a six coordinated octahedral structure of $M(HL^2)_2$ type complexes. In vitro tests for antibacterial and antifungal activities showed that most of the prepared compounds display a good activity towards *S. aureus, E. coli, B. subtilis, P. aureginosa, A. niger, A. flavus, R. stolonifer* and *C. albicans* .

*Corresponding Authors
E-Mail: drrehabalshemary@gmail.com;
maysoontariqwaleed@yahoo.com
[a] Department of Chemistry, College of Education for Pure Sciences / Ibn -Al-Haitham, University of Baghdad

Introduction

Schiff bases and their complexes, containing azomethine nitrogen atom coordinated to metals, belong to a widely studied ligands with high biological activity such as anticancer, antifungal, antibacterial and antimalarial activities.[1-3] Transition metal complexes containing 4-aminoantipyrine and its derivatives have shown a wide range of biological activity, for example copper complexes derived from 4-aminoantipyrine enhances DNA cleavage.[4-11]

Schiff-base complexes belong to the main type of compounds used in the development of "stereochemical models" of coordination chemistry due to their structural diversity. Bidentate and multidendate ligands containing imine groups could be used as modulators of structural and electronic properties of transition metal centers.[12,13]

In the present work, an NN bidendate Schiff base ligand, ((Z)-4-(4-amino-1,5-dimethyl-2-phenyl-1H-pyrazol-3(2H)-ylidene-amino)benzoic acid (HL^1) and an NNO tridendate Schiff base ligand, (4-((E)-4-((E)-((R)-2-hydroxy-1,2-diphenylethylidene)amino)-1,5-dimethyl-2-phenyl-1H-pyrazol-3(2H)-ylideneamino)benzoic acid (H_2L^2) and theirs complexes formed by their reaction with copper(II), nickel(II), cobalt(II), manganese(II) and mercury(II) chlorides ($M(HL^1)_2Cl_2$ and $M(HL^2)_2$ types, respectively) were synthesized and characterized.

Materials and Methods

4-Aminoantipyrine, 4-aminobenzoic acid, benzoin, and the metal(II) chlorides were purchased from Merck. Anhydrous grade methanol and DMSO were purified according to standard procedures. Microanalytical data, ^1H-NMR and ^{13}C-NMR spectra of the compounds were recorded on a Bruker Specrospin Ultrashield Magnets 300 MHz instrument using tetramethylsilane (TMS) as internal standard and DMSO-d_6 as solvent. FT-IR spectra in the range of 4000-400 cm^{-1} were recorded using KBr disk on a SHIMADZUFT-IR 8300 spectrophotometer. UV-Vis spectra were recorded on a Varian Uv-Cary-100 spectrophotometers by using DMSO as solvent. The chloride content of complexes was determined using potentiometric titration method with using 686–Titro Processor–665 Dosim A–Metrohm (Switzerland) instrument. Solid state magnetic susceptibility measurement were performed at room temperature using a Bruker BM6 instrument. Microanalysis (C, H, and N) of the synthesized compounds was carried out using a Perkin Elmer 2400 series analyzer. Melting points were determined in Gallen Kamp melting point apparatus and were uncorrected.

In vitro antimicrobial and antifungal activities assay were performed by well diffusion method. Ethanol was used as a solvent. The Schiff base and its complexes were tested against bacteria such as gram(-) *Bacillus subtilis*, *Escherichia Coli*, *Pseudomonas aureginosa*, gram (+) *Staphylococcus aureus* and antifungal activities of all compounds were studied against four fungal cultures such as *A. niger*, *A. flavus*, *R. stolonifer* and *C. albicans*, cultured on agar as medium. In a typical procedure, a well was made on the agar medium inoculated with bacteria or fungi. The well was filled with the test solution using a micropipette and the plate was incubated

at 37 ℃ for 24 h. During this period, the test solution diffused and the growth of the inoculated bacteria and fungi were affected. The inhibition zone developed on the plate was measured. The inhibitory concentration (MIC) values of the compounds were determined by serial dilution technique.

Synthesis of Schiff bases

Synthesis of the (Z)-4-(4-amino-1,5-dimethyl-2-phenyl-1H-pyrazol-3(2H)-ylideneamino)benzoic acid (HL^1)

An ethanolic solution (50 mL) of 4-aminoantipyrine (0.01 mol, 2.03 g) and 4-aminobenzoic acid (0.01 mol, 1.37g) were refluxed for 36 h after addition of 3-4 drops of glacial acetic acid. The mixture was filtered, the resulting solution was concentrated to (20 mL) on a water bath. On cooling the reaction mixture, sharp yellow crystals product separated out (yield 85 %, m.p. 240 ^{0}C) which was collected by filtration and washed thoroughly with ethanol and then dried in vacuum. The purity of product was checked by TLC method and characterized by elemental and spectral analysis.

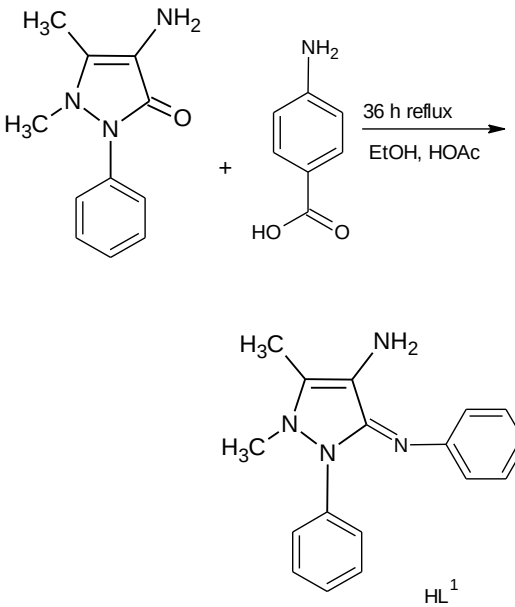

HL^1

Synthesis of 4-((*E*)-4-((*E*)-((*R*)-2-hydroxy-1,2-diphenylethylidene)amino)-1,5-dimethyl-2-phenyl-1*H*-pyrazole-3(2*H*)-ylideneamino)benzoic acid (H_2L^2)

An ethanolic solution (50 mL) of Schiff base (HL^1) (0.01mol, 3.62 g) and benzoin (0.01 mol, 1.37 g) were mixed and refluxed at 70 ^{0}C for 6-7 h after adding anhydrous potassium carbonate. The mixture was filtered and the resulting solution was evaporated to 20 mL on a water bath. The product was filtered off, washed thoroughly with ethanol and subsequently dried at ambient temperature. The purity was confirmed by TLC (yield 82 % , m.p.>280 ^{0}C).[15]

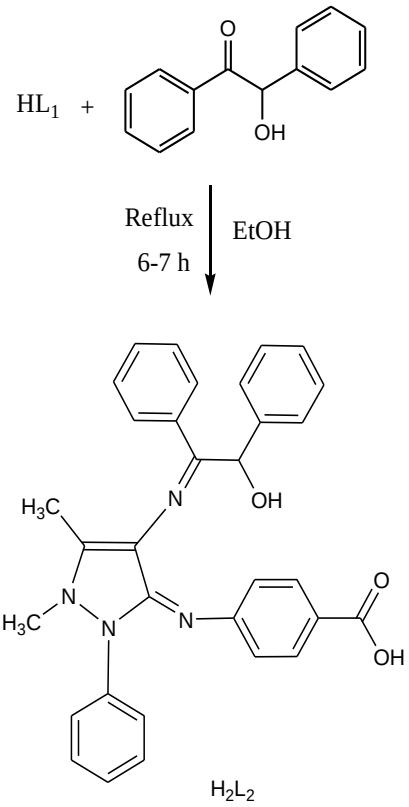

H_2L_2

Synthesis of metal complexes

The solutions of the hydrated chloride salts and $HgCl_2$ (0.001 mol) and the Schiff base ligands (HL^1or H_2L^2) (0.002 mol) in ethanol (50 mL) was refluxed for 1 h. The solution was evaporated to 15 mL and the mixture was cooled to room temperature. The solid complex formed was removed by filtration, washed with hot ethanol until the filtrate becomes colourless. The resulting product was recrystallized from EtOH and dried in a vacuum desiccator over anhydrous $CaCl_2$ (yields = 70-85 %).

Results and Discussion

The analytical values for the ligands (HL^1 and H_2L^2) and their complexes together with some physical characteristics are outlined in table 1. The analytical data of the complexes confirm the general formula $[M(HL^1)_2]Cl_2$ for HL^1 = $C_{18}H_{18}N_4O_2$ and $[M(HL^2)_2]$ for H_2L^2 = $C_{32}H_{28}N_4O_3$ ligands, where M = Cu(II), Ni(II), Co(II), Mn(II) and Hg(II).

All the metal complexes are coloured solids, stable in air at room temperature. The ligands are soluble in most of the organic solvents and all the complexes found to be insoluble in water and freely soluble in methanol and ethanol, $CHCl_3$, DMF and DMSO. The metal complexes exhibit 1:2 (metal-ligand) stoichiometry of the type $[M(HL^1)_2]Cl_2$ and $[M(HL^2)_2]$ where HL^1 acts as bidentate and HL^2(1-) acts as a tridentate ligand.

Table 1. Physical characterization data of the Schiff base ligands ($HL_1$and H_2L_2) and their complexes

Comp.	Molecular formula	Color	Yield %	MP, ^{0}C	Elemental analysis %, Found(calculated)			
					C	H	N	M
HL_1	$C_{18}H_{18}N_4O_2$	yellow	85	232	67.27(67.07)	5.43(5.63)	16.93(17.3)	------
$[Co(L^1)_2]Cl_2$	$C_{36}H_{36}Cl_2CoN_8O_4$	blue	78	265	55.30(55.73)	4.21(4.68)	14.54(14.47)	7.54(7.58)
$[Ni(L^1)_2]Cl_2$	$C_{36}H_{36}Cl_2NiN_8O_4$	green	91	270	55.27(55.67)	4.22(4.69)	14.54(14.47)	7.14(7.58)
$[Cu(L^1)_2]Cl_2$	$C_{36}H_{36}Cl_2CuN_8O_4$	Black	69	310	55.09(55.49)	4.51(4.66)	14.24(14.38)	6.88(7.13)
$[Mn(L^1)_2]Cl_2$	$C_{36}H_{36}Cl_2MnN_8O_4$	Brown	74	282	55.87(56.11)	4.61(4.71)	14.4(14.59)	7.54(7.89)
$[Hg(L^1)_2]Cl_2$	$C_{36}H_{36}Cl_2HgN_8O_4$	Colourless	88	295	46.92(47.14)	3. 63(3.96)	1213(12.23)	12.54(12.89
H_2L^2	$C_{32}H_{28}N_4O_3$	Pale brown	82	245	73.83(74.40)	5.13(5.46)	10.59(10.85)	------
$[Co(L^2)_2]$	$C_{64}H_{54}CoN_8O_6$	Dark brown	85	276	70.24(70.52)	4.73(4.99)	9.87(19.28)	5.63(5.41)
$[Ni(L^2)_2]$	$C_{64}H_{54}NiN_8O_6$	Dark brown	78	267	70.28(70.53)	4.70(4.99)	9.83(10.28)	5.59(5.39)
$[Cu(L^2)_2]$	$C_{64}H_{54}CuN_8O_6$	Dark brown	70	298	70.17(70.22)	4.75(4.82)	9.76(9.88)	5.46(5.32)
$[Mn(L_2)_2]$	$C_{64}H_{54}MnN_8O_6$	Dark brown	74	252	70.09(70.77)	4.65(5.01)	9.92(10.32)	5.31(5.06)
$[Hg(L^2)_2]$	$C_{64}H_{54}HgN_8O_6$	Dark brown	76	213	61.86(62.41)	4.63(4.42)	8.78(9.10)	16.00(16.28)

IR spectra

In order to study the binding mode of the Schiff bases in the complexes, IR data of the ligands and complexes have been compared (Table 2). The peaks appearing in the region of 3444-3359 cm^{-1} are assigned to the uncoordinated O-H stretchings of the ligand (alcoholic and carboxylate OH) in the complexes.

The ligand L^1 shows the characteristic -C=N- band at 1637-1625 cm^{-1} and two NH_2 bands at 3336 and 3215cm^{-1}, which shifts in the complexes to the range 3423 ~ 3305 cm^{-1} and 3371~3209 cm^{-1}, while in the ligand L^2 two peaks of characteristic -C=N- bands appear at 1647~1616 cm^{-1}, which are shifted toward lower frequencies in the spectra of complexes (1638~1589 cm^{-1}). The metal coordination causes appearing of new frequencies in the range 482~450 cm^{-1} and 594~570 cm^{-1}, which are assigned to the fashioning of M-O and M-N bonds, respectively.[7,8] It can thus be concluded that the ligand HL^1 acts as bidendate neutral unit with NN coordination mode, while the ligand H_2L^2 behaves as anionic tridentate unit and coordination to the metal ion through deprotonated alcoholic oxygen and via the two azomethine nitrogen atoms of the Schiff base.

NMR spectra

^{1}H-NMR (DMSO-d_6) of HL^1: δ = 2.26 (3H, -C-CH_3), 2.47 (DMSO), 3.11 (3H, =N-CH_3), 4.95 (2H, -NH_2), 6.5-8.12 (5H, m, C_6H_5), 12.83 (1H, COOH).[9]

^{1}H-NMR (DMSO-d_6) of H_2L^2: δ = 2.26 (1H, OH in benzoin), 2.37 (3H, -C-CH_3), 2.479 (DMSO), 2.53 (3H, -N-CH_3), 5.21 (1H, -C<u>H</u>-OH), 6.4-7.98 (5H, m, C_6H_5), 12.82 (1H, COOH).[10]

^{13}C-NMR (DMSO-d_6) of HL^1: δ = 10.12 (=C-CH_3), 33.70 (-N-CH_3), 40.38 (DMSO), 106.14 (-N-CH_3), 115.38 (-C-CO), 123.56-149.97 (m, C_6H_5), 161.17 (-C=O), 165.79 (C=N).[11]

^{13}C-NMR (DMSO-d_6) of H_2L^2: δ = 10.12 (=C-CH_3), 33.70 (-N-CH_3), 40.38 (DMSO), 75.66 (-C-OH), 106.08 (=C-N), 115.34 (-C-CO), 123.57-149.54 (m, C_6H_5), 161.17-162.54 (-C=N groups), 165.79 (COOH).[12]

Electronic absorption spectra

UV-Vis spectra provide the most detailed information about the structure. Electronic spectrum of the HL^1 ligand displays two bands at 37453 cm^{-1} and 28571 cm^{-1} attributed to π–π* and n–π* transitions. In the spectrum of the complexes of HL^1, the bands observed at range 35714-34722 cm^{-1} and 29154-27548 cm^{-1} are assigned ligand field and LMCT charge transfer transitions. Weak and broad peaks can be shown in the spectrum of the complexes at 23870-14104 cm^{-1} and are assigned to the d-d transitions. The cobalt(II) complex showed one band from d-d transition at 17982 cm^{-1} which may be assigned to $^1A_1 \rightarrow {}^1B_1$transiton in case of tetrahedral environment around the Co^{2+} ion. The magnetic moment of Co(II) complex was found to be 3.9 B.M. which is at the lower end of magnetic moments expected for tetrahedral Co(II) complex.[13]

The absorption spectrum of copper complex showed a band at about 18635 cm^{-1}attributed to $^2B_2 \rightarrow {}^2A_1$ transition of a Cu-complex with tetrahedral geometry. The magnetic moment (μ_{eff}) for this complex was found to be 2.2 B.M. per Cu ion which was in usual range for tetrahedral copper complex.[14]

Table 2. Infrared spectral data(ύ wave number) cm^{-1} for the ligands (HL^1, H_2L^2) and their complexes.

Compound	υ(OH)	υ(NH_2)	υ(C-H) aromatic	υ(C-H) aliphatic	υ(C=O) carboxylic	υ(C=N) imine	υ(C=C)	υ(C-O)	υ(M-N) υ (M-O)
L^1	3444	3336 3215	3051	2970	1668	1597	1566	----	----
$[Co(L^1)_2]Cl_2$	3441	3413 3371	3062	2954	1665	1588	1563	-----	610 464
$[Ni(L^1)_2]Cl_2$	3445	3423 3371	3011	2904	1667	1589	1562	-----	582 443
$[Cu(L^1)_2]Cl_2$	3447	3394 3236	3066	2975	1666	1592	1559	-----	624 462
$[Mn(L^1)_2]Cl_2$	3456	3305 3243	3078	2981	1666	1590	1546	-----	555 451
$[Hg(L^1)_2]Cl_2$	3459	3367 3209	3070	2993	1666	1587	1558	-----	612 466
L^2	2800-3240	---	3059	2904	1668	1600 1658	1587	1165	----
$[Co(L^2)_2]$	3419	---	3105	2976	1667	1638 1618	1565	1205	570 478
$Ni(L^2)_2]$	3407	----	3109	2964	1665	1623 1597	1559	1189	574 468
$[Cu(L^2)_2]$	3429	----	3127	2976	1666	1629 1618	1561	1193	594 468
$[Mn(L^2)_2]$	3444	----	3121	2988	1668	1620 1589	1560	1185	582 482
$[Hg(L^2)_2]$	3402	----	3111	2996	1663	1643 1624	1556	1176	578 442

The electronic spectra of the Ni(II) complex showed bands at 23870 cm^{-1} and 17233 cm^{-1} that may be assigned to the $^1A_1 \rightarrow {}^1A_2$ and $^1A_1 \rightarrow {}^1B_1$ transitions, indicating a tetrahedral environment around the nickel(II) metal ions.

The peak at 14104 cm^{-1}, which may be assigned to $^6A_1 \rightarrow {}^4E_{(G)}$, transition is characteristic for tetrahedral Mn(II) complexes.[15] The magnetic moment of manganese(II) complex is 5.70 B.M. which suggest that the complex is four coordinated.

The electronic spectrum of free Schiff base (H_2L_2) showed two bands at 36363 cm^{-1} and 32362 cm^{-1} due to $\pi \rightarrow \pi^*$ and $n \rightarrow \pi^*$ transitions. In the spectrum of the complexes, these bands observed at the range 36496-35842 cm^{-1} and 31250-30303 cm^{-1}, which are assigned to ligand field and charge transfer (LMCT) transitions.

UV-Vis spectrum of the cobalt(II) complex of H_2L_2 showed the d-d transition bands at 10710, 15943 and 22765 cm^{-1}, which are assigned to $^4T_1g_{(F)} \rightarrow {}^4A_2g_{(F)}$, $^4T_1g_{(F)} \rightarrow {}^4A_2g_{(F)}$ and $^4T_1g_{(F)} \rightarrow {}^4T_1g_{(P)}$ transitions, respectively. These transitions correspond to the octahedral configuration of the complex, which is also supported by the magnetic moment value (4.86 µB) of the complex.[16]

The electronic spectrum of the copper (II) complex displayed in the region of 13523 cm^{-1}. This transition may be attributed to the charge transfer band or the d–d transition band which of $^2Eg \rightarrow {}^2T_2g$ transition. This d–d transition band supports a distorted octahedral configuration around the metal ion, which is also supported by its magnetic moment value (1.66 µB).[17]

The UV-Vis spectrum of the nickel(II) complex shows d–d peaks at 10309, 15587 and 26130 cm^{-1} due to $^3A_2g_{(F)} \rightarrow {}^3T_1g_{(F)}$, $^3A_2g_{(F)} \rightarrow {}^3T_2g_{(F)}$ and $^3A_2g_{(F)} \rightarrow {}^3T_1g_{(P)}$ transitions, respectively, indicating an octahedral geometry. This configuration is further supported by its magnetic moment value (2.89 µB).[18]

The electronic spectrum of Mn(II) complex shows an absorption peak at17605 cm^{-1} assigned to d–d electronic transition type $^6A_1g \rightarrow {}^4T_1g_{(G)}$ which suggests octahedral geometry around Mn(II). This geometry is further supported by the magnetic susceptibility value (5.64 µB).

The complex of Hg(II) is diamagnetic. According to the empirical formula, the same octahedral geometry might be supposed for this complex as well.[19]

Molar conductivity

The molar conductivities of 10^{-3} M of ethanol solution at room temperature were measured. The molar conductivity data of Co(II), Cu(II), Ni(II), Mn(II), and Hg(II) chelates of HL^1 were found to be 72, 77, 86, 82 and 88 $ohm^{-1}\ cm^2\ mol^{-1}$, respectively. It is obvious from these data that these chelates are ionic in nature and they belong to the type of 1:2 electrolytes.[20]

In addition the low conductance values of Co(II), Cu(II), Ni(II), Mn(II), and Hg(II) chelates of H_2L^2 lie in the range 1.2-2.9 $ohm^{-1}\ cm^2\ mol^{-1}$showing their non-ionic nature.

Table 3. Electronic spectral data of the ligands and their metal complexes

Compounds	μ_{eff}	Λ_m, ohm.cm^2 molar^{-1}	Absorption band (nm, cm $^{-1}$)	Transition	Proposed structure
L^1	-	-	267 nm (37453cm^{-1}) 350 nm (28571cm $^{-1}$)	π→π* n→π*	--
$[Co(L^1)_2]Cl_2$	3.9	72	297 nm (33670cm^{-1}) 371 nm (26954cm^{-1}) 556nm (17982cm^{-1})	F.T C.T $^1A_1 \rightarrow {}^1B_1$	Tetrahedral
$[Cu(L^1)_2]Cl_2$	2.2	77	280 nm (35714cm^{-1}) 363 nm (27548cm^{-1}) 536 nm (18635cm^{-1})	F.T C.T $^2B_2 \rightarrow {}^2A_1$	Tetrahedral
$[Ni(L^1)_2]Cl_2$	3.4	86	288 nm (34722cm^{-1}) 368 nm (27173 cm^{-1}) 418.nm (23870 cm^{-1}) 580nm (17233 cm^{-1})	F.T C.T $^1A_1 \rightarrow {}^1A_2$ $^1A_1 \rightarrow {}^1B_1$	Tetrahedral
$[Mn(L^1)_2]Cl_2$	5.70	82	282nm (35460 cm^{-1}) 360 nm (27777cm $^{-1}$) 709 nm(14104 cm^{-1})	F.T C.T $^6A_{1\,(F)} \rightarrow {}^4E_{\,(D)}$	Tetrahedral
$[Hg(L_1)_2]Cl_2$	Dia	88	343 nm (29154 cm $^{-1}$) 432 nm (23148cm $^{-1}$)	F.T C.T	Square planar
L^2	-	-	275 nm (36363 cm $^{-1}$) 309 nm (32362 cm $^{-1}$)	π→π* n→π	----
$[Co(L^2)_2]$	5.42	1.2	278 nm (35971 cm $^{-1}$) 322 nm (31055cm $^{-1}$) 439nm (22765 cm $^{-1}$) 627nm (15943 cm $^{-1}$) 933nm (10710 cm $^{-1}$)	F.T C.T $^4T_1g_{(F)} \rightarrow {}^4T_2g_{(P)}$ $^4T_1g_{(F)} \rightarrow {}^4A_2g_{(F)}$ $^4T_1g \rightarrow {}^4T_2g_{(F)}$	Octahedral
$[Cu(L^2)_2]$	1.81	1.8	279 nm (35842cm $^{-1}$) 322 nm (31055cm $^{-1}$) 739nm(13523 cm^{-1})	F.T C.T $^2Eg \rightarrow {}^2T_2g$	Octahedral
$[Ni(L^2)_2]$	3.23	2.9	275 nm (36363cm $^{-1}$) 328 nm (30487cm $^{-1}$) 970nm (10309 cm^{-1}) 641nm (15587 cm^{-1}) 382nm (26130 cm^{-1})	F.T C.T $^3A_2g_{(F)} \rightarrow {}^3T_1g_{(F)}$ $^3A_2g_{(F)} \rightarrow {}^3T_2g_{(F)}$ $^3A_2g_{(F)} \rightarrow {}^3T_1g_{(P)}$	Octahedral
$[Mn(L^2)_2]$	5.72	2.0	277nm (36101cm $^{-1}$) 330 nm (30303cm^{-1}) 568 nm (17605cm^{-1})	F.T C.T $^6A_1g \rightarrow {}^4T_1g_{(G)}$	Octahedral
$[Hg(L^2)_2]$	-	2.6	274 nm (36496cm $^{-1}$) 320 nm (31250cm^{-1}) 414 nm (24154cm^{-1})	F.T C.T C.T	Octahedral

Table 4. Results of antibacterial bioassay (concentration used 100μg mL^{-1} of DMSO). (a) *E. coli*, (b) *S.aurous*(c) *B. subtilis* (d)*P. aeruginosa*, antifungal bioassay (concentration used 200 μg mL^{-1}). *(a)A. niger*(b) *A. flavus* (c)*R. stolonifer* and (d)*C. albicans* .10<: weak; >10: moderate; >16:significant.

Compounds	Bacteria				Fungi			
	(a)	(b)	(c)	(d)	(a)	(b)	(c)	(d)
L^1	2	3	1	1	17	18	20	19
$[Co(L^1)_2]Cl_2$	7	15	11	10	20	23	26	22
$[Cu(L^1)_2]Cl_2$	9	14	12	13	25	27	30	24
$[Ni(L^1)_2]Cl_2$	16	11	17	13	28	30	32	26
$[Mn(L^1)_2]Cl_2$	9	10	14	12	30	24	29	27
$[Hg(L^1)_2]Cl_2$	8	6	12	14	32	32	34	30
L^2	2	3	4	2	33	28	28	32
$[Co(L^2)_2]$	7	15	11	9	30	35	25	34
$[Cu(L^2)_2]$	9	14	9	12	34	27	28	36
$[Ni(L^2)_2]$	14	11	5	6	35	37	26	30
$[Mn(L^2)_2]$	16	10	13	14	31	32	30	32
$[Hg(L^2)_2]$	9	6	11	17	33	31	34	30

Antibacterial and antifungal activities

The ligands and their complexes have been tested for in vitro growth inhibitory activity against gram(+) (*Staphylococcus aureus*) and gram(-) (*Escherichia Coli*, *Bacillus subtilis*, *Pseudomonasaureginosa*) by using well-diffusion process. The minimum inhibitory concentration (MIC) values of the investigated compounds are summarized in Table 4. As it can be seen from the Table 4, the complexes have high antimicrobial and intermediate antifungal activities. The metal complexes have higher antimicrobial activity than the ligands. The increase in antimicrobial activity might be the consequence of easier diffusion of metal complexes and higher cell permeability.[21-23]

Conclusions

Two new Schiff ligands, namely(Z)-4-(4-amino-1,5-dimethyl-2-phenyl-1H-pyrazol-3(2H)-ylideneamino)benzoic acid (HL^1) and 4-((E)-4-((E)-((R)-2-hydroxy-1,2-diphenylethylidene)amino)-1,5-dimethyl-2-phenyl-1H-pyrazol-3(2H)-ylideneamino)benzoic acid (H_2L^2) and their metal complexes were synthesized. Based on the results of molar conductivity, elemental analysis, UV–Vis,^{1}H- and ^{13}C-NMR and FT-IR spectral studies, it si concluded these ligands form $[M(HL^1)_2]Cl_2$ and $[M(L^2)_2]$ type metal complexes, where M=Co(II), Cu(II), Ni(II), Mn(II) and Hg(II).

The metal (II) ions are coordinated by NN mode with involving the imine (H-C=N) and the amine (NH_2)groups in the case of HL_1 and one deprotonated alcoholic O atom and two imine (H-C=N) groups in the case of H_2L_2. UV-VIS spectroscopic and magnetic data show that all complexes are four-coordinated in the case of HL^1 and six-coordinated in the case of H_2L^2 ligands. The synthesized compounds showed strong antibacterial and intermediate antifungal properties. The microbicide actions of complexes are higher than those of the free ligands.

Acknowledgments

Sincere thanks are expressed to the Department of Chemistry, College of Education for Pure Sciences, Ibn-Al-Haitham, University of Baghdad for financial support.

References

[1]Barboiu, C. T.,Luca, M.,Pop, C., Brewster,E., Dinculescu, E. M., *Eur. J. Med. Chem.*, **1996**, *31*, 597.

[2]El-Ansary, A. L., Abdel-Fattah, H. M. and Abdel-Kader, N. S., *J. Coord. Chem.*, **2008**, *61(18)*, 2950–2960.

[3]Reham, H.,Hassan, A., Manal, M., Nehad, A. L., *J. Chem.*,**2013**, *20(13)*, 10.

4Azzellini, M. A. A. Bagatin I. A. and Ferreira, A. M. D. C.,Redox Report, 11, 25 (1996).

[5]Raman,N., Kulandaisamy, A.,S hunmugasundaram, A., Jeyasubramanium, K., *Transitio. Met. Chem.*, 2**001**, *26*, 131–135.

[6]Raman, N., Sakthivel, A., Rajasekaran, K., *Mycobiology*, **2007**, *35(3)*,150–153.

[7]Tabassum, S, Parveen, S., Arjmand, F., *Indian J. Chem.*, **2004**, *43*, 270–277.

[8]Mishra A. P., Pandey, L. R. ,*Indian J. Chem.*, **2005**, *44A*, 1800–1805.

[9]Raman, N. S., Sobha, S. Mitu, L., *J. Saudi Chem. Soc.*,**2013**, *17*, 151–159.

[10]Santos, M. L. P., Faljoni, A. A., Mangrich, A. S., Ferreira, A. M. D. C., *J. Inorg. Biochem.*, **1998**, *71*, 71.

[11]Santos, M. L. P., Bagatin, I. A., Pereira, E. M., Ferreira, A. M. D. C., *J. Chem. Soc. Dalton Trans*., **2001**,838.

[12]Sumathi, A. S., Tharmaraj,P., Sheela,C. D., *Int. J. Inorg. Chem.*, **2011**, 8.

[13]Kalanithi, M.; Rajarajan, M.; Tharmaraj, P., *J. Coord. Chem.*,**2011**, *64*, 1436–1445.

[14]Dharmaraj, N., Viswanathamurthi, P., Natarajan, K., *Transition Met. Chem*., **2001**, *26*, 105–109.

[15]Muna, A. H. ,*Acta Chim. Pharm. Indica*, **2013**, *3(2),* 127-134.

[16]Sharma, R., Samadhiya, P., Srivastava, S. D., Srivastava, S. K., *Org. Commun*., **2011**, *4(2),*42-51.

[17]Suresh, M.S., Praksh,V., *E-J. Chem.,* **2011**, *8(3),* 1408-1416.

[18]Fernandez-Torres, M. J., *Int. J. Chem.,* **2013**, *9(2),* 33-40.

[19]Raman, T. S., Dhaveethuraja, J., Neelakadan, M.A., Banerjee, S., *J. Chilean Chem. Soc*., **2008**, *53(1),* 1450.

[20]Bahl, B. S., Bahl, A., *Elementary Organic Chemistry*, S. Chand and Company Ltd., New Delhi, **1993**, 60-66.

[21]Ergene, E., Sivas, H., Benkli, K., *Turk. J. Biol*., **2010**, *34*, 379-387.

[22]Layla, A. M., Muna, A. H., Methaq S.M., *J. Chem. Chem, Sci*., **2013**, *3*, 48-96.

[23]Gupta, A. K. S., Barhate, V. D., *Res. J. Pharm., Biol. Chem. Sci.*, **2012**, *3(3)*,1014-1020.

[24]Singh, P., Dhakarey, R. K. S., *Rasayan J. Chem*., **2009**, *2(4),* 869-874.

[25]El-Ansary, A. L., Abdel-Kader, N. S., *Int. J. Inorg. Chem*., **2012**, 13.

Received: 27.09.2016.
Accepted: 06.01.2017.

PRODUCTION OF CATHODE MATERIAL FOR OXYGEN ELECTRODES BY ANODIC OXIDIZATION OF MULTIWALL CARBON NANOTUBES

M.O. Danilov[a],*, I.A. Rusetskii[a], I.A. Slobodyanyuk[a], O.Y. Khyzhun[b], G.Ya. Kolbasov[a]

Keywords: Anodic oxidation of carbon nanotubes, Graphene oxide, Electrode materials, Oxygen electrode.

We report the synthesis of graphene oxide by the electrochemical method. The standard redox potentials of the carboxyl groups of carbon is used to select the oxidation potential. Graphene oxide obtained by anodic oxidation of multiwall carbon nanotubes in concentrated sulfuric acid, confirmed by electron microscopy, XRD, X-ray photoelectron spectroscopy, X-ray emission spectroscopy and Raman spectra, is a prospective electrode material for the chemical current sources. The oxidation potential in 96 % sulfuric acid is +3 V and the time of oxidation was 4 h. A good electrical conductivity is observed because of the presence of fragments of carbon nanotube in graphene oxide. Thus, this material is a very promising electrode material for oxygen electrodes. The current–voltage characteristics of the oxygen electrodes, based on electrochemically produced graphene oxide, is the graphene oxide produced by anodic oxidation of multiwall carbon nanotubes.

*Corresponding Author:
E-Mail: danilovmickle@rambler.ru
[a] Vernadskii Institute of General and Inorganic Chemistry, National Academy of Science of Ukraine, 32–34 Palladin Avenue, 03680 Kyiv, Ukraine.
[b] Frantsevych Institute for Problems of Materials Science, National Academy of Sciences of Ukraine, 3 Krzhyzhanivsky Street, 03142 Kyiv, Ukraine.

Introduction

Application of air or oxygen electrodes in devices generating electrical energy is useful; such application does cause environmental problems and allows to save nonrenewable natural resources. The air and oxygen electrode is a three-phase electrode–electrolyte–gas system, where the generation of electric current is localized at a phase boundary. The current magnitude generated at such gas diffusion electrode depends on the triple contact zone of these three phases. In its turn, the electrode itself is composed of catalyst and carrier. The interaction between them determines the quantity of generated current, which depends on catalyst being used. It is known that the most effective catalyst for oxygen recovery is platinum, which is a very expensive material. A great number of workers is forced to study other effective but less expensive catalysts.[1] Another problem is catalytically active and stable carrier. The benefits of carbon nanotubes used as the carrier are shown. [2–4] Presently, a series of stuies have been reported using graphene as an electrode material for lithium-ionic accumulators[5] and also as a catalyst carrier for catalysts in fuel cells.[6–10]

At the moment the methods known for the synthesis of graphene from carbon nanotubes are:[11] intercalation of alkaline earth elements and nitrogen; plasma etching; microwave unzipping; unzipping by catalytic metal nanoparticles; ultrasonic unzipping; opening-up by laser irradiation; electrical unzipping; hydrogenating at the high-temperature; unzipping by influence of a scanning tunneling microscope; electrochemical unrolling; the redox chemical synthesis. Among most technologically advanced methods, in our opinion, electrochemical process is paid much attention because it has the ability to control the process by changing three parameters: voltage, current, and time of this process.

Although extensive studies have been performed to obtain graphene nanosheets via electrochemical exfoliation of graphite,[12] Pillai and his group are unique who suggested that in aqueous electrolytes using electrochemical oxidizing and reducing, longitudinal splitting and unzipping single[13] and multiwall carbon nanotubes (MWNTs)[14] are possible to be synthesized. According to Pillai, inducing electric field at the phase boundary results in the cleavage of carbon-carbon, similar to the mechanism of oxidation of olefin to the diol,[15,16] by forming the complex manganese ester.[17,18] Further, the diol is oxidized to form keto groups and complete rupture of the C = C bonds. Experimental studies,[19] as well as results obtained by Tour and co-workers[20–22] have shown that the unzipping of MWCNTs is most likely due to the intercalation of oxidized molecules in the defects in multi-walled carbon nanotubes.

Formation of surface groups on highly oriented pyrolytic graphite (HOPG) by electrochemical oxidation and intercalation acid anions is described.[23–27] Electro oxidation mechanism was studied in sulfuric acid, and it shows the formation of alcohol and other functional groups on the basal plane of HOPG surface.[25] As a result of oxidation, the surface was hydrophilic for its nature.[28] This phenomenon has been useful for the dispersion of graphene oxide (GO) in deionized water.[29] The use of sulfuric acid leads to a strong oxidation of graphene surfaces to form thin sheets with a large number of the structure defects.[30] High resistivity of graphene oxide is due to defects caused by damages of sp^2-structure.[31]

Graphene is usually obtained as a mixture of mono-, bi- and multilayer (3 – 10 monolayers) structured irregular flakes or plane sheets.[32] Based on the standard redox potentials of carbon[33] (Table 1) the required oxidant potential in acidic medium should be higher than + 0.528 V.

Table 1. Oxidant potentials in acidic and alkaline mediums

Acidic, in V		**Alkaline**	
$C,H^+/ CH_3OH$	–0.320	$C/CH_3OH,OH$	–1.480
$HCO_2H,H^+/C$	+0.528	$CHO_2^{1-}/C,OH^-$	–0.603
$CO,H^+/C$	+0.518	$CO_3^{2-}/C,OH^-$	–0.766
$H_2CO_3,H^+/C$	+0.207		

At the electrochemical oxidation of multi-walled carbon nanotube, electrode potential is more electropositive because of the polarization of the electrode-collector material, the ohmic losses in the MWCNT and kinetic difficulties. This is confirmed by experimental data on the oxidation of MWCNTs in sulfuric acid at potentials between 0.7 and 4.8 V relative to the silver-chloride electrode.[34] In a review,[19] numerous works on the anodic oxidation of different forms of carbon in sulfuric acid at electrodes of various materials at a voltage of 1 to 10 V are discussed. Based on analysis of existing literature data, the possibility of obtaining the graphene oxide by anodic oxidation of multi-walled carbon nanotubes, to the best of our knowledge, has not been attempted as yet.

Based on the above studies it is clear that there is no consensus on the possibility of obtaining the graphene oxide by anodic oxidation of multi-walled carbon nanotubes. Therefore, the aim of this study was to investigate the possibility of obtaining graphene oxide, using carbon nanotubes as a starting material, by simple technology method for the production of the electrode material for the oxygen electrodes of the fuel cells.

Experimental

For the electrochemical production of graphene oxide, multi-walled carbon nanotubes were used. The outer diameter of MWCNTs was about 10 – 30 nm, the specific surface area was 230 $m^2 g^{-1}$, with a bulk density of 25 – 35 g dm^{-3}. The number of walls ranges from 8 to 15. Anodic oxidation of carbon nanotubes was conducted in a 150 ml glass beaker containing 96 % sulfuric acid solution, the weight of MWCNT was 1 g. The container for the oxidation of MWCNT is a bag that served as a membrane in lead accumulators, which is stable in acid, is used. For the firmly pressed MWCNTs to the anode electrodes, PTFE liners were used. Titanium and platinum electrodes are used as cathodes and the anodes respectively. Oxidation of carbon nanotubes was carried out in the galvanostatic mode. A silver-chloride electrode connected through a salt bridge was used as a reference electrode. The samples of graphene oxide (GO) obtained by the electrochemical oxidation of the carbon nanotubes were examined with a JEM–100 CXII electron microscope. The X-ray phase analysis was performed using a DRON–4 X-ray diffractometer employing CuK_α irradiation. Raman spectra of initial MWCNTs and GO were registered by INVIA Raman microscope (Renishaw) under the excitation of He-Ne laser with λ_{ex} = 0.6328 Å. The position of standard Si sample at 520 cm^{-1} was used as the reference for wavenumber calibration. WiRE 3.4 software was used for Raman data acquisition and data analysis. The presence of oxygen-containing groups in graphene oxide was analyzed employing the X-ray photoelectron spectroscopy (XPS) method. The XPS spectra of graphene oxide and, for comparison, pristine multiwall carbon nanotubes (MWCNTs) were recorded using the UHV-Analysis-System designed and assembled by SPECS Surface Nano Analysis Company (Berlin, Germany). The UHV-Analysis-System is supplied with a hemispherical PHOIBOS 150 analyzer. The XPS spectra of the graphene oxide and MWCNTs were recorded in an ion-pumped chamber at a base pressure less than $8 \cdot 10^{-10}$ mbar. The XPS spectra of the above mentioned carbon materials were excited by a MgK_α source of X-ray irradiation (E = 1253.6 eV) and were measured at a constant pass energy of 30 eV. Furthermore, the X-ray emission spectroscopy (XES) method is recognized as a very powerful technique when studying carbon materials[35,36] by measuring the XES CK_α band, which represents the energy distribution of the C 2p states. Technique of recording the XES CK_α band ($K \rightarrow L_{II,III}$ transition) was similar to that described.[37] Briefly, the XES CK_α bands of graphene oxide and MWCNTs were acquired employing an RSM–500 spectrometer-monochromator equipped with a diffraction grating (600 groves / mm, radius of curvature of R = 6026 mm). Secondary electron multiplier VEU–6 with a CsI photocathode was used as a detector. Working condition of a spectrometer electron gun when exciting the XES CK_α bands was set as follows: U_a = 5.0 kV and I_a = 2.2 mA. Energy resolution of the RSM–500 spectrometer was evaluated to be 0.25 eV when measuring the XES CK_α bands of graphene oxide and MWCNTs.

The synthesized materials were prepared by pressing two-layer oxygen electrodes. The hydrophobic layer contained 0.07 g / cm^2 acetylene black with 25 % polytetrafluoroethylene, and the active layer contained 0.02 g / cm^2 RGO, with 5 % polytetrafluoroethylene. The studies were carried out on a fuel cell mockup, a zinc electrode being used as the anode. A mockup for the testing of gas-diffusion electrodes is described.[38] The electrolyte was a 6 M KOH solution. . A silver-chloride electrode connected through a salt bridge was used as a reference electrode. The electrochemical characteristics were recorded under galvanostatic conditions. The oxygen source was a U-shaped electrolyzer with alkaline electrolyte. Oxygen was supplied to the gas electrodes under an excess pressure of 0.01 MPa. Before measurements, the oxygen electrode was blown through with oxygen over an hour.

The characteristics of the oxygen electrode from the electrode materials obtained by the anodic oxidations of carbon nanotubes were compared with the characteristics of electrodes from the initial MWCNT with deposited platinum black. Platinum is deposited by electrochemical method from an aqueous solution containing 3 % H_2PtCl_6 and 0.2 % lead acetate (II) at a voltage of 1 V for 2 min; the current direction is changed through 30 s.

Results and Discussion

We investigated the dependence of the electrochemical characteristics of oxygen electrodes based on the GO obtained by the oxidation of MWCNTs with various time. Anodic oxidation of MWCNT was performed at a potential + 3 V over 1.5, 4, and 5 h. As can be seen from the current–voltage curves plotted for the oxygen electrode (Figure 1), increasing the anodic oxidation time to 4 hours leads to increase of the electrochemical characteristics of the electrodes (Curve 2). With further increase of the time of oxidation the characteristics do not vary significantly (Curve 3).

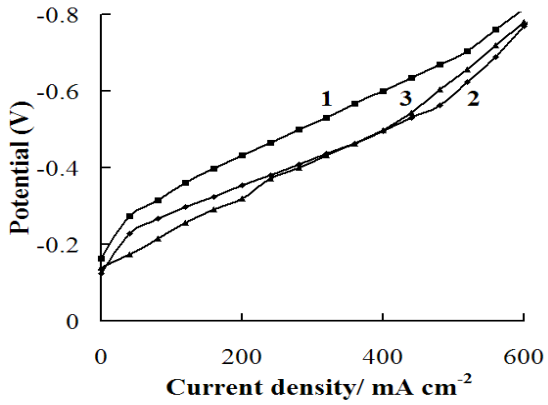

Figure 1. Dependence of potential on current density for oxygen electrodes with the active layer in an amount of 0.02 g / cm^2 consisting of graphene oxide prepared by electrochemical oxidation of MWCNTs at the potential + 3 V with different oxidation time: (1) 1.5, (2) 4 and (3) 5 h.

We have also carried out the oxidation of MWCNTs at the different potentials over 4 hours. Potential ranged from + 1.8 V to + 4.5 V. As shown in Figure 2, the anodic oxidation of multiwalled carbon nanotubes over 4 h at the potential of + 3.0 V produces the most catalytically active materials for oxygen electrode.

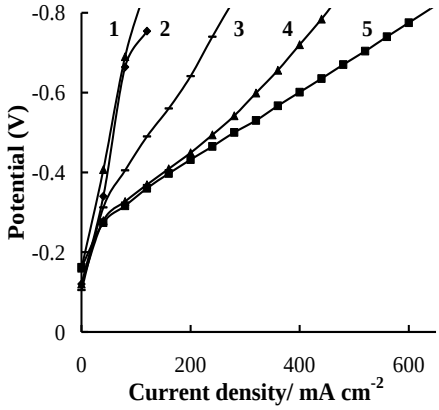

Figure 2. Dependence of potential on current density for oxygen electrodes with the active layer in an amount of 0.02 g / cm^2 consisting of the graphene oxide prepared by electrochemical oxidation of MWNTs at various potentials (V): (1) initial MWCNTs, (2) + 1.8, (3) + 4.5, (4) + 2.5, and (5) + 3.0 V.

Materials obtained by anodic oxidation of MWCNTs were investigated by means of various physical and chemical methods. Figure 3 shows the XRD analysis of the obtained samples.

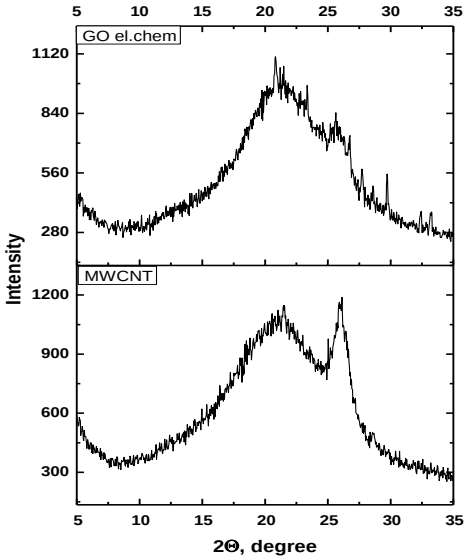

Figure 3. XRD patterns of the samples of initial MWCNTs (MWCNT, bottom panel) and graphene oxide (GO el.chem, upper panel) obtained by electrochemical oxidation of the multi-walled carbon nanotubes.

As one can see from the micrograph presented in Figure 4a, employing the anodic oxidation of carbon nanotubes, we have obtained samples of graphene oxide. Closely spaced tags of the carbon atoms in the diffraction ring, Figure 4b, show that the obtained sample consists of undulating planar multilayer's of graphene oxide. The case of obtaining such graphene is reported. [32] From micrographs, number of layers of graphene oxide was estimated that ranges from 3 to 10. Also, there are fragments of the original multi-walled carbon nanotubes into graphene oxide, which leads to good electrical conductivity of received materials, as opposed to pure graphene oxide. This is evidenced by good electrochemical characteristics of oxygen electrodes obtained in the present work based on graphene oxide (Figures 1 and 2). Figure 5 shows Raman spectra obtained at 633 nm and intensity of 50 % for the graphene oxide prepared by anodic oxidation of MWCNTs in the acidic medium. Analysis of Raman spectra confirms the presence of graphene oxide multilayers.

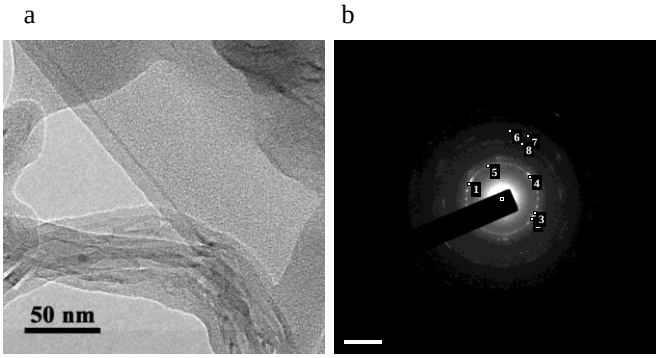

Figure 4. (a) Electron micrograph of graphene oxide obtained by anodic oxidation of MWCNTs, and (b) the diffraction of this sample

Figures 4a and b show an electron micrograph of graphene oxide obtained by electrochemical oxidation of carbon nanotubes and the diffraction of this sample, respectively.

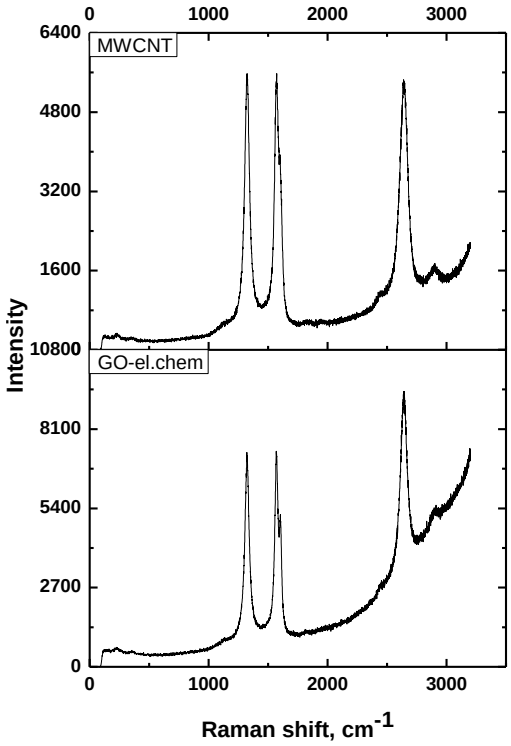

Figure 5. Raman spectra obtained at 633 nm and intensity of 50 % for graphene oxide (GO el.chem, bottom panel) obtained by anodic oxidation of MWNTs and initial MWCNTs (MWCNT, upper panel).

Figure 6 presents the XPS spectra of the graphene oxide and MWCNTs under study. Results of the present XPS measurements indicate that the surface of the pristine MWCNTs reveals the presence of oxygen, with the binding energy of the O 1*s* core level electrons that is equal to 531.9 eV. This binding energy value corresponds to oxygen-containing species adsorbed on the MWCNTs surface due to exposure of the specimen to air for a long time (several weeks). When going from MWCNTs to graphene oxide, the relative intensity of the XPS O^{1s} core-level spectrum increases (Figure 6) and its binding energy decreases by about 0.5 eV (Figure 7). The later effect can be explained by the fact that the XPS O 1*s* core-level spectrum of graphene oxide is a superposition of the spectra of oxygen belonging to adsorbed oxygen-containing species and of oxygen binding with graphene. The precise measurements of the XPS C 1*s* core-level spectra (Figure 7a) allow for concluding that the maxima of the spectra coincide within accuracy of the present measurements (± 0.05 eV) for the both samples under study. Furthermore, it is worth mentioning that binding energies of the maxima of the XPS C^{1s} core-level spectra of the graphene oxide and MWCNTs, as it is evidenced from Figure 7a, are close to that of graphite, namely 284.4 eV.[39]

Figure 8 presents the XES CK_α bands measured for graphene oxide and MWCNTs. It has been reported[40,41] that in the high-energy portion of the XES C Kα band of MWSNTs the π- and $\pi^+\sigma$-binding states are positioned. These states correspond to the fine-structure peculiarities labeled as "c", "d", "e" of the XES CK_α band that are well resolved for the both samples under study (Figure 8). The mentioned states represent the energy distribution of the C^{2p} states involved in the mixed $pp\sigma^+$ / $pp\pi$ and pure $pp\pi$ interactions[40] in the radial planes and along the axis of

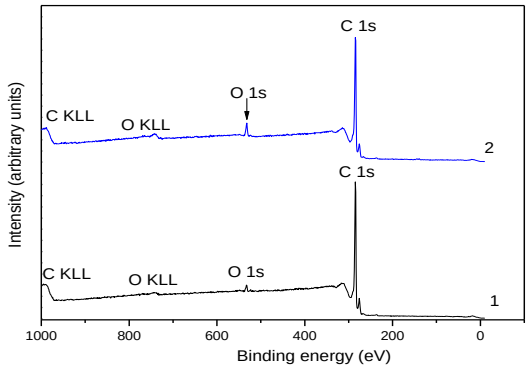

Figure 6. Survey XPS spectra of (1) MWCNTs and (2) graphene oxide.

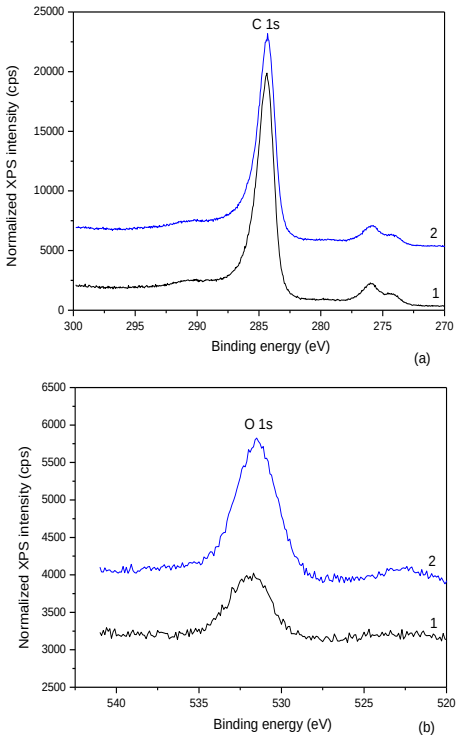

Figure 7. Detailed XPS (a) C 1*s* and (b) O 1*s* core-levels spectra of (1) MWCNTs and (2) graphene oxide

MWCNTs, respectively.[40,41] It is worth indicating that the XES C Kα band derived in the present work for MWCNTs, by its shape and energy positions of the fine-structure peculiarities, resembles the similar bands recorded in Ref.[41] for 200-walled nanotubes with a diameter of 140 nm and double-walled nanotubes with a diameter of 4 nm obtained in arc discharge without catalysts by MER-corporation. In the latter work, it has been established that the bandwidth of the CK_α band of double-walled carbon nanotubes reduces in comparison with that of the 200-walled carbon nanotubes only near the band maximum (at $I > 0.75\ I_{max}$).

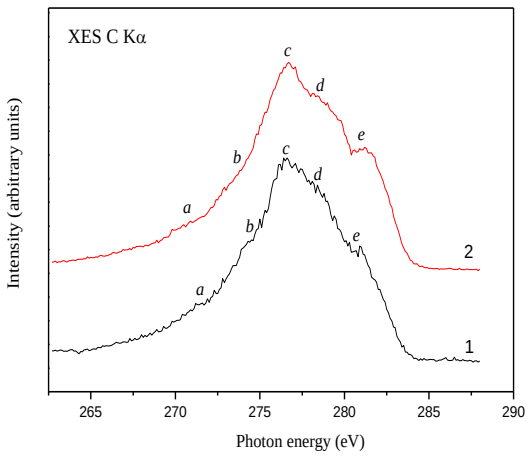

Figure 8. The XES CK$_\alpha$ bands of (1) MWCNTs and (2) graphene oxide.

This effect is explained in Ref.[41] as a result of a decrease of the $\pi^+\sigma$-overlapping in the radial plane inside the 200-walled carbon nanotubes with an increase in diameter of every following wall. As a consequence, the C 2*p* states involved in such bonds shift toward higher photon energies.[41]

As can be seen from Figure 8, when going from MWCNTs to graphene oxide synthesized in the present work, visible changes occur in the shape of the XES CK$_\alpha$ band. In particular, the sub-band "e" of the XES CK$_\alpha$ band appearing due to the existence of the C 2*p* states involved in pure ppπ interactions increases its width in graphene oxide. Furthermore, the maximum "c" of the XES CK$_\alpha$ band, where mixed *pp*σ^+ / *pp*π interactions are located, becomes narrower when going from MWCNTs to graphene oxide.

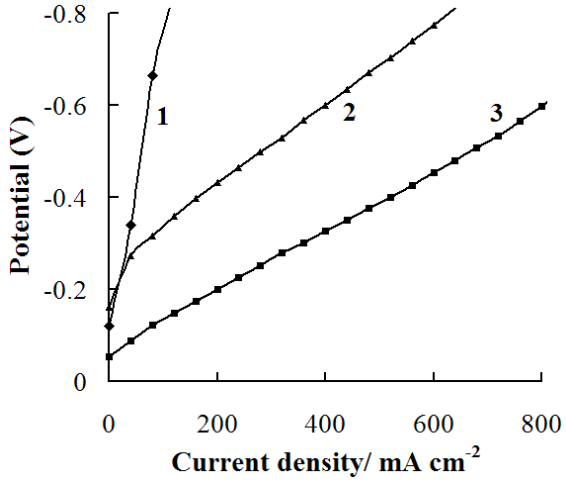

Figure 9. Dependence of potential on current density for oxygen electrodes with the active layer in an amount of 0.02 g / cm^2 consisting of: (1) initial MWCNTs; (2) graphene oxide produced by oxidation of MWCNTs in sulfuric acid for 4 h at an anode potential of + 3.0; (3) MWCNTs with deposited platinum in an amount of 10 wt. %.

Figure 9 shows the comparative characteristics of the oxygen electrodes on the basis of initial MWCNTs (Curve 1), graphene oxide obtained by electrochemical oxidation of MWCNTs (Curve 2) and MWNTs with deposited platinum (curve 3). As one can see from Figure 9, the electrocatalytic characteristics of electrodes based on graphene oxide are close to the characteristics of electrodes based on platinum-containing materials. All examined graphene oxide materials were stable within six months when being tested in the galvanostatic regime in the fuel-element mockup at a current density of 200 mA / cm^2 at oxygen electrodes.

Based on these results, we can conclude that using anodic electrochemical oxidation of multi-walled carbon nanotubes over 4 h in electrolyte of 96 % sulfuric acid at a potential of + 3 V, graphene oxide can be synthesized.

Conclusion

Graphene oxide was synthesized in the present work by anodic oxidation of multi-walled carbon nanotubes. We have determined that the most appropriate conditions for such a synthesis are as follows: oxidation potential in 96 % sulfuric acid is + 3 V and the oxidation duration is 4 h. The formation of well defined graphene oxide was confirmed by data of electron microscopy, X-ray diffraction, X-ray photoelectron spectroscopy, X-ray emission spectroscopy and Raman spectra. In particular, comparative XPS studies of graphene oxide and MWCNTs indicate that the surface of pristine MWCNTs reveals the presence of oxygen, with the binding energy that corresponds to oxygen-containing species adsorbed on the MWCNTs surface due to exposure of the specimen to air for a long time (several weeks). Our XPS data reveal that when going from MWCNTs to graphene oxide, the XPS O 1*s* core-level binding energy decreases by about 0.5 eV that can be explained by the fact that the XPS O 1*s* spectrum of graphene oxide is a superposition of the spectra of oxygen belonging to adsorbed oxygen-containing species and of oxygen binding with graphene. The maxima of the XPS C 1*s* core-level spectra coincide within accuracy of the present measurements (± 0.05 eV) for graphene oxide and MWCNTs under study. However, when going from MWCNTs to graphene oxide, visible changes occur in the shape of the XES CK$_\alpha$ band, representing the energy distribution of the C 2*p* states. In particular, the high-energy sub-band appearing due to the existence of the C 2*p* states involved in pure *pp*π interactions increases its width in graphene oxide, while the main maximum of the XES CK$_\alpha$ band, where mixed *pp*σ^+ / *pp*π states are located, becomes narrower when going from MWCNTs to graphene oxide. Furthermore, due to the presence of fragments of carbon nanotubes in graphene oxide synthesized, the latter reveals good electrical conductivity. Therefore, this material is expected to be a very promising electrode material for oxygen electrodes of power sources.

Acknowledgement

This paper has been presented at the 4th International Conference "Nanotechnologies", October 24 – 27, 2016, Tbilisi, Georgia (Nano – 2016).

References

[1]Bidault, F., Brett, D. J. L., Middleton, P. H., Brandon, N. P., *J. Power Sources*, **2009**, *187*, 39.

[2]Soehn, M., Lebert, M., Wirth, T., Hofmann, S., Nicoloso, N., *J. Power Sources*, **2008**, *176*, 494.

[3]Hsieh, C-T., Lin, J-Yi., Wei, J.-L., *Int. J. Hydrogen Energy*, **2009**, *34*, 685.

[4]Wang, X., Waje, M., Yan, Y., *Electrochem. Solid-State Lett.*, **2005**, *8*, A42.

[5]Wang, G., Shen, X., Yao, J., Park, J., *Carbon*, **2009**, *47*, 2049.

[6]Xin, Y., Liu, J., Jie, X., Liu, W., Liu, F., Yin, Y., Gu, J., Zou, Z., *Electrochim. Acta*, **2012**, *60*, 354.

[7]Lin, Z., Waller, G., Liu, Y., Liu, M., Wong, C. P., *Adv. Energy Mater.*, **2012**, *2*, 884.

[8]Qu, L. T., Liu, Y., Baek, J. B., Dai, L. M., *ACS Nano*, **2010**, *4*, 1321.

[9]Lin, Z. Y., Song, M. K., Ding, Y., Liu, Y., Liu, M. L., Wong, C. P. , *Phys. Chem. Chem. Phys.*, **2012**, *14*, 3381.

[10]Shao, Y., Zhang, S., Wang, C., Nie, Z., Liu, J., Wang, Y., Lin, Y., *J. Power Sources*, **2010**, *195*, 4600.

[11]Danilov, M. O., Slobodyanyuk, I. A., Rusetskii, I. A., Kolbasov, G. Ya., in: Aliofkhazraei, M., Ali, N., Milne, W. I., Ozkan, C. S., Mitura, S., Gervasoni J. L. (Eds.), *Graphene Science Handbook. Fabrication Methods*, CRC Press/Taylor & Francis**, 2016**, 205.

[12]Low, C. T. J., Walsh, F. C., Chakrabarti, M. H., Hashim, M. A., Hussain, M. A., *Carbon*, **2013**, *54*, 1.

[13]John, R., Shinde, D. B., Liu, L., Ding, F., Xu, Z., Vijayan, C., Pillai, V. K., Pradeep, T., *ACS Nano*, **2014**, *8*, 234.

[14]Shinde, D. B., Debgupta, J., Kushwaha, A., Aslam, M., Pillai, V. K., *J. Am. Chem. Soc.*, **2011**, *133*, 4168.

[15]Waters, W. A., *Quart. Rev. Chem. Soc.*, **1958**, *12*, 277.

[16]Ohloff, G ., Giersch, W., *Angew. Chem., Int. Ed. Engl.*, **1973**, *12*, 401.

[17]Kosynkin, D. V., Higginbotham, A. L., Sinitskii, A., Lomeda1, J. R., Dimiev, A., Price, B. K., Tour, J. M., *Nature*, **2009**, *458*, 872.

[18]Higginbotham, A. L., Kosynkin, D. V., Sinitskii, A., Sun, Z., Tour, J. M., *ACS Nano*, **2010**, *4*, 2059.

[19]Low, C. T. J., Walsh, F. C., Chakrabarti, M. H., Hashim, M. A., Hussain, M.A., Carbon, 2013, 54, 1.

[20]Dimiev, A. M., Tour, J. M., *ACS Nano*, **2014**, *8*, 3060.

[21]James, D. K., Tour, J. M., *Acc. Chem. Res.*, **2013**, *46*, 2307.

[22]James, D. K., Tour, J. M., *Macromol. Chem. Phys.*, **2012**, *213*, 1033.

[23]Hathcock, K. W., Brumfield, J. C., Goss, C. A., Irene, E. A., Murray, R. W., *Anal. Chem.*, **1995**, *67*, 2201.

[24]Skowronski, J. M., *Synth. Metal.*, **1995**, *73*, 21.

[25]Bourelle, E., Claude-Montigny, B., Metrot, A., *Mol. Cryst. Liq. Cryst.*, **1998**, *310*, 321.

[26]Alliata, D., Haring, P., Haas, O., Kotz, R., Siegenthaler, H., *Electrochem, Commun.*, **1999**, *1*, 5.

[27]Schnyder, B., Alliata, D., Kotz, R., Siegenthaler, H., *Appl. Surface Sci.*, **2001**, *173*, 221.

[28]Choo, H. S., Kinumoto, T., Jeong, S. K., Iriyama, Y., Abe, T., Ogumi, Z., *J. Electrochem. Soc.*, **2007**, *154*, B1017.

[29]Dilimon, V. S., Sampath, S., *Thin Solid Films*, **2011**, *519*, 2323.

[30]Su, C. Y., Lu, A. Y., Xu, Y., Chen, F. R., Khlobystov, A. N., Li, L. J., *ACS Nano*, **2011**, *5*, 2332.

[31]You, X., Chang, J. H., Ju, B. K., Pak, J. J., *J. Nanosci. Nanotechnol.*, **2011**, *11*, 5965.

[32]Yan, L., Zheng, Y. B., Zhao, F., Li, S., Gao, X., Xu, B., Weiss, P. S., Zhao, Y., *Chem. Soc. Rev.*, **2012**, *41*, 97.

[33]Bratsch, S. G., *J. Phys. Chem.*, **1989**, *18*, 1.

[34]Zehtab, A. Y., Roberts, E. P. L., Sundararaj, U., *Mat. Research Bull.*, **2016**, *80*, 243.

[35]Meisel, A., Leonhardt, G., Szargan, R., *X-Ray Spectra and Chemical Binding, Springer-Verlag, Berlin/Heidelberg*, **1989**.

[36]Kurdyumov, A. V., Britun, V. F., Khyzhun, O. Y., Zaulychnyy, Y. V., Bekenev, V. L., Dymarchuk, V. O., Danilenko, A. I., *Diamond Relat. Mater.*, **2011**, *20*, 974.

[37]Khyzhun, O. Y., Zhurakovsky, E. A., Sinelnichenko, A. K., Kolyagin, V. A., *J. Electron Spectrosc. Relat. Phenom.*, **1996**, *82*, 179.

[38]Danilov, M. O., Kolbasov, G. Ya., Rusetskii, I. A., Slobodyanyuk, I. A., *Russ. J. Appl. Chem.*, **2012**, *85*, 1536.

[39]Khyzhun, O. Y., *J. Alloys Compd.*, **1997**, *259*, 47.

[40]Östling, D., Tománek, D., Rosén, A., *Phys. Rev. B*, **1997**, *55*, 13980.

[41]Zaulychnyy, Y.V., Solonin, Y.M., Foya, O.O., Khyzhun, O.Y., Vasylkiv, O., *Metallofiz. Noveishie Tekhnol.*, **2008**, *30*, 169.

Received: 27.11.2016.
Accepted: 06.01.2017.

MITOCHONDRIAL UNCOUPLING CARRIER PROTEIN-2 DNA POLYMORPHISM (−866 G/A) AS A RISK FOR POLYCYSTIC OVARY SYNDROME IN SAUDI ARABIAN FEMALES

Mohamed A. Taher*[a], Mohra Taher Hasseb[b] and Ahmed I. Abd Elneam[c]

Keywords: polycystic ovary syndrome; single nucleotide polymorphism; type 2 diabetes; obesity.

Polycystic ovary syndrome (PCOS) is a common hormonal disorder characterized by gonadotropin dysregulation, hyperandrogenism, menstrual irregularity and ovarian morphology. The uncoupling protein-2 (UCP-2) gene is a member of the mitochondrial anion carrier protein (MACP) and is strongly associated with insulin resistance and obesity. An attempt is made to detect the association between PCOS and -866G/A polymorphism in UCP2 gene promoter. The study is carried on forty-seven patients with polycystic ovary syndrome and fifty–six controls. Blood samples were taken for biochemical tests and restriction fragment length polymorphism (RFLP) for detection of -866 G/A UCP2 gene polymorphisms. Significant associations between the -866A/A -866G/A of UCP2 gene promotor and PCOS are reported including a significant association between -866A/A polymorphism of UCP2 and both obesity (high BMI) and type 2 diabetes.

* Corresponding Author
E-Mail: abdelmoaty5@yahoo.com
[a] Biochemistry Department, Faculty of Medicine, Sohag University, Egypt.
[b] Gynealogical . and Obst. Department, El-Dawadmy General Hospital, KSA.
[c] Molecular Genetics and Enzymology Dept., Human Genetics Division, National Research Centre, 33 El Bohouth St. (former El Tahrir St.), Dokki 12622, Cairo, Egypt

Introduction

Polycystic ovary syndrome (PCOS) is the most common endocrinal disorder among reproductive age of women and has multiple features such as menstrual irregularity, hyperandrogenism, gonadotropin dysregulation, and ovarian morphology in the overall phenotype[1]. In addition to its reproductive features, it is associated with an increased risk of overweight or obesity, diabetes mellitus (type 2) and insulin resistance.[2]

Uncoupling protein-2 (UCP2) is a member of the mitochondrial transporter protein carrier (MTPC) and is located in the inner mitochondrial membrane.[3] It is a member of the larger family of mitochondrial anion carrier proteins (MACP).[3] It separates oxidative phosphorylation from synthesis of adenosine triphosphate (ATP) with energy release as heat (mitochondrial proton leak) and results in reduced ATP synthesis.[3] It helps the transfer of anions from inner to outer mitochondrial membrane and the return of the protons in the reverse direction from the outer to the inner mitochondrial membrane.[4] Therefore, it decreases the mitochondrial membrane potential.[4] It may have a role in thermogenesis, obesity, diabetes and atherosclerosis.[5] Now it appears that the main UCP2 function is the controlling of mitochondria reactive oxygen species. UCP-2 has three homologous protein domains.[6]

UCP2 gene is located at chromosome 11 q13.4 and expressed in many tissues, with the greatest expression in skeletal muscle,[7] and adipose tissue.[8] G/A polymorphism of the UCP2 promoter at position -866 varied in different populations.[9] G allele (wild type) is associated with reduction of mRNA expression in adipose tissue with low risk of obesity in the middle-aged humans and low risk of T2D.[10] UCP2 -866G/A polymorphism contributes to abnormal insulin hormone secretion and glucose tolerance in Italian population.[11] The same results were found in young German subjects.[12] The UCP2 is one of the responsible gene for T2D and obesity.[5] The distribution of UCP2 polymorphism in the healthy Caucasians and Iranian population is different from the Japanese population.[13]

The aim of the present study was to analyze the association between PCOS in Saudi Arabian females and -866G/A SNP of the UCP2 gene polymorphism.

Forty-seven patients with polycystic ovary syndrome were selected from outpatient's clinics of Al-Dawadmie hospital KSA from November 2015 to February 2016. The diagnosis of PCOS was made according to Rotterdam criteria (2003) which depends on present two of the three criteria needed to be fulfilled for the diagnosis of PCOS (1) clinically associated features (hirsutism or acne) and/or high serum androgen levels (2) irregular menstrual cycle (3) ultrasonographic finding of polycystic ovarian.[14] Fifty-six females without PCOS criteria were selected as control.

Complete physical, laboratory and genetic examinations were done to both groups. Local Medical Ethical Committee approved this study ethically and a written informed consent was taken from both control subjects and patients.

Experimentals

Mitochondrial DNA extraction

Mitochondrial DNA was purified from whole blood samples with the QIAamp® DNA Blood Mini Kit (Holliston, MA, USA). DNA was eluted in 150 µl elution buffer and examined on 1% agarose gel and stored at – 20°C for analysis.

PCR and restriction fragment length polymorphism (PCR-RFLP)

DNA fragment corresponding to the UCP2 G (−866) A polymorphism (rs659366) was amplified by 5'-CAC GCT GCT TCT GCC AGG AC-3' as forward primer and 5'-AGG CGT CAG GAG ATG GAC CG-3' as reverse primer.[15]

PCR products were digested by MluI restriction enzyme (NEB, Ipswich, MA, USA) and separated on 2% agarose gel electrophoresis.[16] The −866A/A genotype was marked by a single 363 bp fragment due to loss of MluI site (Figures. 1 and 2), while the wild-type (−866) G/G genotype was digested into 295 and 68 bp fragments (Fig. 2). (−866) A/G genotype was digested into 363, 295 and 68 bp fragments. 68 bp band does not present in (-866G/G), and (-866A/G) in the Figure 2.

Biochemical determinations

Blood samples from the PCOS patients and controls were analyzed using biochemical assays, including FSH (Human FSH EIA Test Kit Catalog No: 40-052-115017 GENWAY BIOTECH IN), LH (Ultra Sensitive Luteinizing Hormone (LH) LumELISA Catalog No. 40-101-325027 GENWAY BIOTECH IN), TSH (Thyroid Stimulating Hormone (TSH) Human ELISA Kit (Abcam), PRL (PRL human ELISA KIT KA0217 Catalog No (Abnova), DHEA-S (DHEA sulfate (DHEA-S) ELISA Kit (ab108669) (Abcam) and E2 (Prostaglandin E2 High Sensitivity ELISA Kit (ab133055) Abcam).

Anthropometry assessment

Anthropometric evaluation was performed for all the patients in both groups. Body weight, height and waist circumference were measured.[17] Waist circumference was measured at the level of the umbilicus with the standing position, the face directed forward, shoulders relaxed; and normal breathing by using non-stretchable plastic tape to the nearest 0.1 cm. Body mass index (BMI) was calculated as body weight divided by height squared (kg m^{-2}).

Statistical analysis

Allele's frequency and genotypes were computed using the Arlequin software (version 3.1) and SNP stats (http://bioinfo.iconcologia.net/SN Pstats). Data were presented by means ± SD and percentages. The compiled data were computerized and analysed by SPSS V 12. The following tests of significance were used: t-test between means we used to analyse mean difference, t-test between percentage to analyse percent difference and chi–square. A level of $p < 0.05$ was considered significant.

Results

A total of 47 polycystic ovary syndrome patients and 56 control subjects were included in this study. General and clinical characteristics of all the subjects enrolled in this study are shown in Table 1. Patients with significantly high serum TSH, LH, testosterone and DHEA-S in PCO than control subjects were observed.

Comparing -866G/A polymorphism of UCP2 gene and alleles in PCOS Patients and controls were tabulated (Tables 2 and 3). The -866 A/A and A/G UCP2 gene polymorphisms and -866 A allele were significantly higher in PCOS than control group. Relations of -866G/A polymorphism of UCP2 gene and both $HbA1_c$ (Table 4) and BMI (Table 5) were shown that -866 A/A UCP2 gene polymorphism was significantly higher in both uncontrolled DM (Table 4) and obesity (Table 5).

Table 1. General and clinical characteristics of PCOS and control groups

Parameters	Control subjects (mean ± SD)	PCOS patients (mean ± SD)
Age (years)	34.6 ±12.3	37.7 ±13.9
Mean BMI	22.54 ± 1.4	26.31±2.6*
Waist/hip ratio	0.82±0.06	0.99 ±0.032
E2 levels (ng mL^{-1})	32.7 ±14.7	22.9±19.4
Prolactin levels (ng mL^{-1})	16.4±4.8	16.8 ±6.7
Testosterone (ng mL^{-1})	0.32 ±0.12	0.59 ±0.18*
DHEA-S level (µg mL^{-1})	129.5±24.2	200±34.3*
TSH levels (µIU mL^{-1})	1.44 ±0.6	1.39 ±0.7
FSH levels (µIU mL^{-1})	5.1 ±3.9	6 ±3.3
LH levels (µIU mL^{-1})	4.3±2.1	9 ±1.4*
LH/FSH	0.8 ±0.5	1.5 ±0.4*

*Significant change ($p< 0.05$) between PCOS subjects and controls

Table 2. Distribution of -866 G/A polymorphism in PCOS patients and controls

Parameters	Control subjects (*n*=56)	PCOS Patients (*n*=47)
-866 AA(*n*,%)	16 (28.5%)	15 (32%)*
-866 AG(*n*,%)	10 (18%)	22(47%)*
-866 GG(*n*,%)	30 (53.5%)*	10 (21%)

*Significant change ($p<0.05$) between PCOS subjects and controls

Table 3. Distribution of -866 G/A alleles in PCOS patients and controls

Parameters	Control subjects (*n*=112)	PCOS patients (*n*=94)
-866 A (*n*,%)	42 (37.5 %)	52 (55 %)*
-866 G (*n*,%)	70 (62.5 %)*	42 (45 %)

*Significant change ($p<0.05$) between PCOS Subjects and controls.

Table 4. Relation between HbA1c and -866 (G/A) genotypes

Parameters	HbA1c≤ 7% *n*=71	HbA1c>7% *n*=32
-866 AA (*n*, %)	18 (25.4 %)	13 (40.6 %)*
-866 AG (*n*, %)	22 (31 %)	10(31.3 %)
-866 GG *n* (%)	31 (43.7%)	9 (28.1%)

*Significant change ($p<0.05$) between PCOS subjects and controls.

Table 5. relation between BMI and -866 (G/A) genotypes

Parameters	BMI ≤ 25 n (65)	BMI > 25 n (38)
-866 AA (*n*, %)	15(23.1%)	16 (42.1%)*
-866 AG (*n*, (%)	20 (30.8%)	12 (31.6%)
-866 GG (*n*, %)	30 (46.2%)*	10 (26.3%)

*Significant change ($p < 0.05$) between PCOS Subjects and controls.

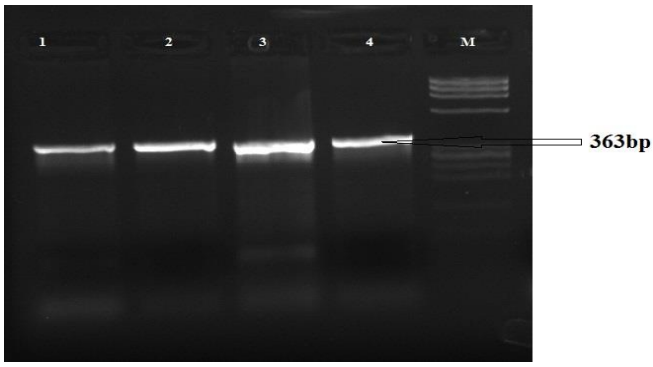

Figure 1. PCR amplification for −866A/A polymorphism UCP2 gene: Lanes 1, 2, 3 and 4 PCR product with length 360 base pair. Lane M ϕx 147 marker.

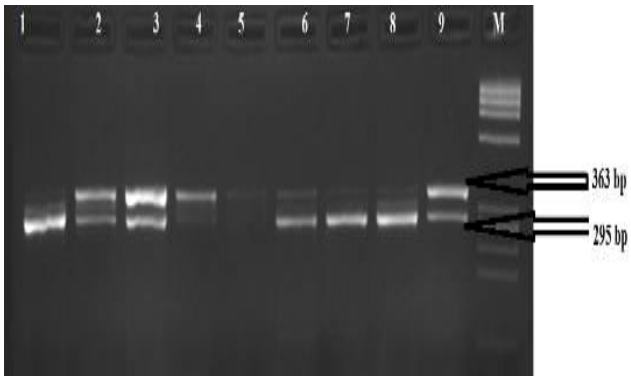

Figure 2. Restriction enzyme analysis for −866G/G and −866G/A polymorphisms of UCP2 gene PCR: Lanes 1, 6, 7 and 8 with 295 bp (-866G/G), lanes 4 and 5 with 363 bp (-866A/A) and lane 2, 3, and 9 with 363bp and 295 bp (-866A/G). Lane M ϕx 147 marker.

Discussion

Polycystic ovary syndrome (PCOS) is a common cause of female infertility during reproduction period associated with production of surplus of androgens causing irregular ovulation, or even a lack of ovulation[18]. Androgens are responsible for body changes in male like muscle mass and hair growth. In women, androgens are necessary to make estrogen.[18] In the current research, PCOS women have significantly high androgen levels. The excess androgen in women with PCOS can cause acne and excessive hair growth.[18]

Excess androgen production in case of PCOS also leads to irregular or absent ovulation[19]. In the current research, PCOS women have significantly high serum LH/FSH (more than 1). Because of its anovulatory effect, PCOS women may have difficulty in getting pregnant.[19]

Many PCOS women are resistant to insulin action. This means that they need larger than normal amounts of insulin to maintain normal blood sugar levels.[2] These women are at high risk for diabetes. In the current study, PCOS women have significantly high serum $HbA1_c$. High insulin levels caused by insulin resistance can lead to excessive production of androgen[3]. Beside the reproductive disorders in PCOS there are an association with an increased risk of obesity[7] and T2D.[5] In our study, PCOS women have significantly high BMI.

Several genetic studies of PCOS were caarried out and it wwas found that many genetic region were associated with it such as CAPN10 (calpain 10),[20] CYP11A (cytochrome P450, family 11, sub family A),[21] the insulin gene VNTR (variable number of tandem repeats),[22] and D19S884 (di nucleotide repeat marker mapping to chromo some 19p13.2).[23] In the present study, UCPs has a key role in the regulation of human energy production by uncoupling respiration from oxidative phosphorylation, and thus converting stored energy to free heat.[24] UCP-2 -866G/A SNP was identified in the promoter region.[25-27]. This polymorphism was reported in fat metabolism, diabetes and obesity,[28&29] UCP-2 -866A/A gene allele was frequently reported not only with increased adipose mRNA expression and obesity[30-32] but also, with type 2 diabetes (T2D) secondary to reduction in insulin potency.[30] UCP-2 -866G/A gene alleles were reported to have a low risk of coronary artery disease,[33] very low energy levels in the peripheral nerve function,[34] high risk of metabolic syndrome, higher waist-to-hip ratio[35] and higher serum oxidative stress markers.[36] UCP-2 -866G/G gene allele was shown to be associated with a reduced mRNA expression in adipose tissue, low BMI,[37] decrease risk of obesity[28], high insulin sensitivity and a reduced risk of T2D.[26] These genotype form were reported to have low blood triglyceride levels[37] and higher levels of LDL-cholesterol.[34] UCP-2 -866A/A and -866G/A genotype is assumed that the UCP2 gene is associated with obesity and type 2 diabetes, it is also associated with obesity in females with PCOS.

In conclusion, there are a significant association between the -866A/A and -866G/A gene polymorphisms in the UCP2 gene promoter and PCOS in Saudi Arabian females. The -866A/A polymorphism of UCP2 is associated with (high BMI) obesity and T2D in the same study group. Further investigations for studying -866G/A polymorphism of the UCP2 gene promotor and PCOS patients on a large scale or in different ethnic groups is required.

Acknowledgments

The authors are very grateful to patients and their family for their participation and cooperation during this study. We did not get funds from any funding body for this study. We again thank their ethical committee for approving the work.

Conflict of Interests

The authors declare that there is no conflict of interests regarding the publication of this paper.

References

[1] Klein, J., Craven,, M., Vuguin, P. M., *Adolesc. Med. State Art Rev*., **2015**, *26(2)*, 326-42.

[2]Ali, A. T., *Ceska Gynekol*., **2015**, *80(4)*, 279-89.

[3]Toda, C., Diano, S., *Best Pract. Res. Clin. Endocrinol. Metab*., **2014**, *28(5)*, 757-64.

[4]Hoshovs'ka, I. V., *Fiziol. Zh*., **2015**, *61(1)*, 91-101.

[5]Zee, R. Y., Ridker, P. M., Chasman, D. I., *Atherosclerosis*, **2011**, *214(1)*, 107-9.

[6]Seli, E., Horvath, T. L., *Rev. Endocr. Metab. Disorders*, **2013**, *14(4)*, 347-50.

[7]Pheiffer, C., Jacobs, C., Patel, O., Ghoor, S., Muller, C., *Louw. J*., **2016**, *72(1)*:25-32.

[8]Mahadik, S. R., Lele, R. D., Saranath, D., Seth, A., Parikh, V., *Adipocyte*, **2012**, *1(2)*, 101-107.

[9]Pheiffer, C., Jacobs, C., Patel, O., Ghoor, S., Muller, C., Louw, J., *J. Physiol. Biochem*., **2016**, *72(1)*, 25-32.

[10]Maestrini, S., Podestà, F., Di Blasio, A. M., Savia, G., Brunani, A., Tagliaferri, A., Mencarelli, M., Chiodini, I., Liuzzi, A., *J Endocrinol. Invest*., **2003**, *26(10)*, 985-90.

[11]Mancini, F. P., Sabatino, L., Colantuoni, V., Pasanisi, F., Finelli, C., Contaldo, F., Masulli, M., Riccardi, G., Vaccaro, O., *Clin. Endocrinol. (Oxford)*, **2003**, *59(6)*, 817-22.

[12]Labayen, I., Ortega, F. B., Sjöström, M., Nilsson, T. K., Olsson, L. A., Ruiz, J. R., *Pediatr. Res*., **2009**, *66(3)*, 350-4.

[13]Heidari, J., Akrami, S. M., Heshmat, R., Amiri, P., Fakhrzadeh, H., Pajouhi, M., *Arch. Iran Med*., **2010**, *13(5)*, 384-90.

[14]The Rotterdam ESHRE/ASRM-Sponsored PCOS consensus workshop group, *Hum. Reprod*., **2004**, *19*, 41–47

[15]Sesti, G., Cardellini, M., Marini, M. A., Frontoni, S., D'Adamo, M., Del Guerra, S., Lauro, D., De Nicolais, P., Sbraccia, P., Del Prato, S., Gambardella, S., Federici, M., Marchetti, P., Lauro, R,. *Diabetes*, **2003**, *52*, 1280–1283.

[16]Oktavianthi, S., Trimarsanto, H., Febinia, C. A., Suastika, K., Saraswati, M. R., Dwipayana, P., Arindrarto, W., Sudoyo, H., Malik, S. G., *Cardiovasc. Diabetol*., **2012**, *11*, 41.

[17]Szmodis, M., Bosnyák, E., Protzner, A., Szőts, G., Trájer, E., Tóth, M., *Anthropol. Anz*., **2016**, *73(1)*, 23-32.

[18]Liu, Y., Jiang, H., Xing, F. Q., Huang, W. J., Mao, L. H., He, L. Y., *Endocrine*, **2013**, *43(3)*, 714-23.

[19]Kumar, A. N., Naidu, J. N., Satyanarayana, U., Ramalingam, K., Anitha, M., *Int- J. Steril*., **2016**, *10(1)*, 22-8.

[20]Dasgupta, S., Sirisha, P. V., Neelaveni, K., Anuradha, K., Reddy, B. M., *PLoS One*., **2012**, *7(2)*, e32192.

[21]Urbanek, M., *Nat. Clin. Pract. Endocrinol Metab*., **2007**, *3(2)*, 103-11.

[22]Attaoua, R.., Boeckler, N., Radian, S., Ait El Mkadem, S., Poucheret, P., Latapie, V., Gheorghiu, M., Fica, S., Vintila, M., Normand, C., Coculescu, M., Grigorescu, F., *Endokrynol. Pol*., **2015**, *66(3)*, 198-206.

[23]Ackerman, C. M., Lowe, L. P., Lee, H., Chen, F., Hughes, E., Cholod, P., Dyer, A. R., Hayes, M. G., Metzger, B. E., Lowe, W. L., Urbanek, M., *J. Clin. Endocrinol. Metab*., **2010**, *95(7)*, 3242-50.

[24]Chan, C. B., and Kashemsant, N., *Biochem. Soc. Trans*., **2006**, *34*, 802-805.

[25]Saleh, M. C., Wheeler, M. B., Chan, C. B., *Diabetologia*., **2002**, *45*, 174-187.

[26]Wang, H., Chu, W. S., Lu, T., Hasstedt, S. J., Kern, P. A., Elbein, S. C., *Am. J. Physiol. Endocrinol. Metab*., **2004**, *286*, E1-E7.

[27]Heidari, J., Akrami, S. M., Heshmat, R., Amiri, P., Fakhrzadeh, H., Pajouhi, M., *Arch. Iran Med*., **2010**, *13*, 384-390.

[28]Krempler, F., Esterbauer, H., Weitgasser, R., Ebenbichler, C., Patsch, J. R., Miller, K., Xie M., Linnemayr, V., Oberkofler, H., Patsch, W., *Diabetes*, **2002**, *51*, 3331-3335.

[29]Jia, J. J., Zhang, X., Ge, C. R., Jois, M., *Obes. Rev*., **2009**, *10*, 519-526.

[30]Caro, J. F., *J. Clin. Endocrinol. Metab*., **1991**, *73*: 691-695.

[31]Palmer, B. R., Devereaux, C. L., Dhamrait, S. S., Mocatta, T. J., Pilbrow, A. P., Frampton, C. M., Skelton, L. Y., Andle, T. G., Winterbourn, C. C., Richards, A. M., Montgomery, H. E., Cameron, V. A., *Cardiovasc. Diabetol*., **2009**, *8*, 31.

[32]Cheurfa, N., Dubois-Laforgue, D., Ferrarezi, D. A., Reis, A. F, Brenner, G. M., Bouché, C., Le Feuvre, C., Fumeron, F., Timsit, J., Marre, M., Velho, G., *Diabetes*, **2008**, *57*, 1063-1068.

[33]Yamasaki, H., Sasaki, H., Ogawa, K., Shono, T., Tamura, S., Doi, A., Sasahara, M., Kawashima, H., Nakao, T., Furuta, H., Nishi, M., Nanjo, K., *Diabetes Care*, **2006**, *29*, 888-894 .

[34]Shen, H., Qi, L., Tai, E. S., Chew, S. K., Tan, C. E. Ordovas, J. M., *Obesity*, **2006**, *14*, 656-661.

[35]Stephens, J. W., Dhamrait, S. S., Mani, A. R., Acharya, J., Moore, K., Hurel, S. J., Humphries, S. E., *Nutr. Metab. Cardiovasc. Dis*., **2008**, *18*, 7-14.

[36]Yoon, Y., Park, B. L., Cha, M. H., Kim, K. S., Cheong, H. S., Choi, Y. H., Shin, H. D., *Biochem. Biophys. Res. Commun*., **2007**, *359*, 451-456. .

[37]Reis, A. F., Dubois-Laforgue, D., Bellanne-Chantelot, C., Timsit, J., Velho, G., *Mol. Genet. Metab*., **2004**, *82*, 339-344.

Received: 01.12.2016.
Accepted: 10.01.2017.

SYNTHESIS AND CHARACTERIZATION OF γ-LACTAMS THROUGH IMINE INTERMEDIATES

Assala Salam Jebur[a] and Mahmood Shakir Magtoof[a]*

Keywords: γ- lactams, imines, NMR.

This study is concerned with the synthesis and characterization of γ-lactams (**3a-3h**). γ-Lactams were prepared by reacting phenylsuccinic anhydride with the appropriate Schiff bases (imines) by heating at 51-61 °C in chloroform with moderate yields (51-75 **%**). The structures of these compounds were established on the basis of the spectral studies using IR, ^{1}H-NMR, ^{13}C-NMR , ^{13}C- NMR DEPT and MS.

Corresponding Authors
Tel: 009647813199256
E-Mail: Mahmood672000@yahoo.com
[a] Department of Chemistry, Science, College,Thiqar University, Thiqar, Nashyria , Iraq

Introduction

2-Oxopyrrolidine γ-lactam is five-membered ring lactams (Figure 1). γ-Lactams exist in many natural products and biologically active compounds and are one of the most important classes of compounds for drug discovery.[1-3] Substituted γ-lactams, in particular, have potential application in drug synthesis, but the development of stereoselective synthesis of chiral γ-lactams remains a challenge.[4,5] Developing effective and simple synthetic methods is important so that the drug candidates can be screened.

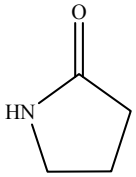

Figure 1. γ-Lactam ring

Stereoselective addition to a γ-lactam skeleton provides a direct and efficient method for synthesizing various γ-lactam derivatives. However, the most commonly used methods for synthesizing chiral γ-lactams are based on the cyclization or cycloaddition of N-containing precursors, which are synthesized stereoselectively, and there are limited studies on the stereoselective additions to γ-lactam skeletons. [6-8]

Experimental

The ^{1}H-NMR spectra were recorded using VARIAN spectrophotometer (500 MHz), the ^{13}C-NMR spectra were recorded using VARIAN spectrophotometer (75 MHz).The chemical shift values are expressed in δ (ppm), using tetramethylsilane (TMS) as internal standard and DMSO-d_6 as solvent. The mass spectra were recorded at 3 kV.

Preparation of mono-imines (2a-2d)

In general, the mono-imines (**2a-2d)** are prepared by the reaction of the mixture of 0.01 mole amine with 0.01 mol aldehyde in 25 mL of methanol or ethanol and 4-6 drops of glacial acetic acid, the reaction mixture is refluxed with stirring for 0.5-9 h, the progress of the reaction is followed by TLC using hexane : ethyl acetate (6:4) as eluent. After completion, the solvent evaporates and then recrystallizes from a suitable solvent.[9-11]

(E)-3-((4-Bromophenyl)imino)indolin-2-one (2a)

The compound was prepared by reacting 1.169 g (0.01 mol) of 4-bromoaniline and 1 g (0.01 mol) of indoline-2,3-dione. Yield 75 %, m.p. 273-275 ºC, colour orange, IR (KBr disk) 1608 cm^{-1} (C=N).

(E)-2-(((4-Bromophenyl)imino)methyl)-6-ethoxyphenol (2b)

The compound was prepared by reacting 1.036 g (0.01 mol) of 4-bromoaniline and 1.169 g (0.01 mol) of 3-ethoxy-2-hydroxybenzaldehyde. Yield 79 %, m.p. 89-90 ºC, colour orange, IR (KBr disk) 1681 cm^{-1} (C=N).

(E)-4-Bromo-2-(((4-nitrophenyl)imino)methyl)phenol (2c)

The compound was prepared by reacting 0.68g (0.01 mol) of 4-nitroaniline and 1 g (0.01 mol) of 5-bromo-2-hydroxybenzaldehyde. Yield 69 %, m.p. 178-180 ºC, colour yellowish, IR (KBr disk) 1618 cm^{-1} (C=N).

(E)-4-Bromo-2-((naphthalen-1-ylimino) methyl)phenol (2d)

The compound was prepared by reacting 0.71g (0.01 mol) of naphthalen-1-amine and 1 g (0.01 mol) of 5-bromo-2-hydroxybenzaldehyde. Yield 87.5 %, m.p. 105-106 ºC, colour maronite, IR (KBr disk) 1620 cm^{-1} (C=N).

Preparation of bis-imines (2e-2g)

In general, the bis-imines (**2e-2g**) are prepared by the reaction of 0.01 mole diamine with 0.02 mole of aldehyde

in 25 mL of methanol or ethanol and 4-6 drops of glacial acetic acid, the reaction mixture is refluxed for 1-9 h, the progress of the reaction is followed by TLC using hexane : ethyl acetate 6:4 as eluent. After completion, the solvent was evaporated and the product was then recrystallized from a suitable solvent.

6,6'-((1E,1'E)-((Methylenebis(4,1-phenylene)) bis(azanylidene)) bis(methanylylidene))bis(2-ethoxyphenol) (2e)

The compound was prepared by reacting 0.595 g (0.01 mol) of 4,4'-methylenedianiline with 1g (0.02 mol) of 3-ethoxy-2-hydroxybenzaldehyde. Yield 87.6 %, m.p.157-158 ºC, colour yellowish, IR (KBr disk)1624 cm^{-1} (C=N).

6,6'-((1E,1'E)-(Naphthalene-1,5-diylbis(azanylylidene))-bis(methan ylylidene))bis(2-ethoxyphenol) (2f)

The compound was prepared by reacting 0.452 g (0.01 mol) of 1,5-diaminonaphthalene with 0.95 g (0.02 mol) of 3-ethoxy-2-hydroxybenzaldehyde .Yield 96 %, m.p. 133-136ºC, colour chartreuse, IR (KBr disk)1618 cm^{-1} (C=N).

(N1E,N5E)-N1,N5-Bis(4-chlorobenzylidene)naphthalen-e-1,5-diamine (2g)

The compound was prepared by reacting 0.562 g (0.01 mol) of 1,5-diaminonaphthalene with1 g (0.02mol) of 4-chlorobenzaldehyde. Yield 96.5 %, m.p. 190-192ºC, colour green, IR (KBr disk) 1621 cm^{-1} (C=N).

General procedure for the preparation of γ-lactams 3a-3g

Preparation of mono-γ-lactams 3a-3d.

In general, the mono-γ- lactams (**3a-3d)** were prepared by reacting a mixture of 0.01 mol of monoimine (**2a-2d**) with 0.01 mol of phenylsuccinic anhydride in 25 mL of chloroform and heating the mixture in water bath at 51-61 °C. The reaction mixture was then refluxed for 12-30 h with stirring. The progress of the reaction was followed by TLC. After completion, the solvent was evaporated, and the residue was recrystallized from a suitable solvent. [12-13]

1'-(4-Bromophenyl)-2,5'-dioxo-3'-phenylspiro[indoline-3, 2'-pyrrolidine]-3'-carboxylic acid (3a)

The compound was prepared by reacting 0.5 g (0.01 mol) of **2a** with 0.292 g (0.01 mol) of phenylsuccinic anhydride. Yield 51 %, m.p. 192-195 ºC, colour orange. IR (KBr): 1650 cm^{-1} (HO–C=O), 1721 cm^{-1} (–N–C=O).^{1}H-NMR (500 MHz, DMSO) δ = 3.3 (s, 2H, γ-Lactam ring), 7.2-8.21 (m, 13H, Ar-H), 9.4 (s, 1H, -NHC=O), 11.3 (s, 1H, OHC=O). ^{13}C-NMR (75 MHz, DMSO) δ = 48 (s, C_4H), 52(-C_2-), 58(s, C_3-H), 116-151 (m, C-Ar), 174 (s, CH_2-C=O), 175(s, HN-C=O), 179(s, HO-C=O).

1-(4-Bromophenyl)-2-(3-ethoxy-2-hydroxyphenyl)-5-oxo-3-phenylpyrrolidine-3-carboxylic acid (3b)

The compound was prepared by reacting 0.8 g (0.01mol) of **2b** with 0.43 g (0.01 mol) of phenylsuccinic anhydride. Yield 74 %, m.p. 83-85 ºC, colour orange. IR (KBr): 1656 cm^{-1} (HO–C=O), 1722 cm^{-1} (–N–C=O). ^{1}H-NMR (500 MHz, DMSO) δ = 3.6 (s, 2H, C_4-H), 3.8 (s, 2H, CH_2-O), 1.78 (3H, -CH_3), 7.72 - 8.28 (m, 12H, Ar-H), 4.02 (s, 1H, C_2-H), 10.8 (s, 1H, OHC=O), 9.6 (s, 1H, Ar-OH). ^{13}C-NMR (75 MHz, DMSO) δ = 29 (s, -CH_3), 42 (s, -CH_2-), 44 (s, CH_2-O), 49 (s, -CH-), 59 (s, -COOH), 115-158 (m, C-Ar), 173 (s, CH_2-C=O), 180 (s, HO-C=O).

2-(5-Bromo-2-hydroxyphenyl)-1-(4-nitrophenyl)-5-oxo-3-phenylpyrrolidine-3-carboxylic acid (3c)

The compound was prepared by reacting 0.8 g (0.01mol) of **2c** with 0.438 g (0.01 mol) of phenylsuccinic anhydride. Yield 65 %, m.p. 110-112 ºC, colour yellow. IR (KBr): 1682 cm^{-1} (HO–C=O), 1725 cm^{-1} (–N–C=O). ^{1}H-NMR (500 MHz, DMSO) δ = 3.7 (s, 2H, C_4-H), 4.1 (s, 1H, C_2-H), 7.28-8.15 (m, 12H, Ar-H), 11.0 (s, 1H, OHC=O), 9.4 (s, 1H, Ar-OH).^{13} C-NMR (75 MHz, DMSO) δ = 44 (s, -CH_2-O), 46 (s, CH_2-), 52 (s, -CH-), 57 (s, COOH), 120-156 (m, C-Ar), 181 (s, HO-C=O), 178 (s, CH_2-C=O).

2-(5-Bromo-2-hydroxyphenyl)-1-(naphthalen-1-yl)-5-oxo-3-phenylpyrrolidine-3-carboxylic acid (3d)

The compound was prepared by reacting 0.6 g (0.01 mol) of **2d** with 0.323g (0.01 mol) of phenylsuccinic anhydride. Yield 69 %, m.p. 190-192 ºC, colour brown. IR (KBr):1690 cm^{-1} (HO-C=O), 1721 cm^{-1} (–N–C=O). ^{1}H-NMR (500 MHz, DMSO) δ = 3.7 (s, 2H, C_4-H), 4.3 (s, 1H, C_2-H), 7.20-8.52 (m,15H, Ar-H), 10.9 (s, 1H, OHC=O), 9.6 (s, 1H, Ar-OH).^{13} C-NMR (75 MHz, DMSO) δ = 42 (s, -CH2-O), 45 (s ,-CH_2), 53(s, -CH-), 56 (s, -COOH), 112-154 (m, C-Ar), 175 (s, HO-C=O), 178(s, CH_2-C=O).

Preparation of bis-γ-lactams (3e-3g)

In general, the bis-γ-lactams (**3e-3g**) were prepared by reacting 0.01 mol bis-imines (**2e-2g**) with 0.02 mol of phenylsuccinic anhydride in 25 mL of chloroform under heating in water bath at 51-61 °C. The reaction mixture was refluxed for 12-16 h with stirring. The progress of the reaction was followed by TLC. After completion, the solvent was evaporated and the residue was recrystallized from a suitable solvent.

1,1'-(Methylenebis(4,1-phenylene))bis(2-(3-ethoxy-2-hydroxyphenyl)-5-oxo-3-phenylpyrrolidine-3-carboxylic acid) (3e)

The compound was prepared by reacting 0.5 g (0.01 mol) of **2e** with 0.385 g (0.02 mol) of phenylsuccinic anhydride. Yield 73 %, m.p. 172-173 ºC, colour orange. IR (KBr): 1654 cm^{-1} (HO-C=O), 1733 cm^{-1} (–N–C=O).

^{1}H-NMR (500 MHz, DMSO) δ = 1.78 (s, 6H, -CH_3), 3.6 (s, 4H, C_4-H), 3.85 (s, 2H, -CH_2-), 4.1 (s, -CH_2-),7.2-8.58 (m, 24H, Ar-H), 9.4 (s, 2H, Ar-OH), 10.73 (s, 2H, OHC=O).[13] C-NMR (75 MHz, DMSO) δ = 41 (d, -CH_2-O), 29 (d, -CH_3),31 (s, Ar-CH_2-Ar), 42 (d, -CH_2-), 57 (d, -CH-), 55 (d, -COOH), 111-158 (m, C-Ar),171 (d, CH $_2$-C=O), 173 (d, HN-C=O),178 (d, HO-C=O).

1,1'-(Naphthalene-1,5-diyl)bis(2-(3-ethoxy-2-hydroxyphe-nyl)-5-oxo-3-phenylpyrrolidine-3-carboxylic acid) (3f)

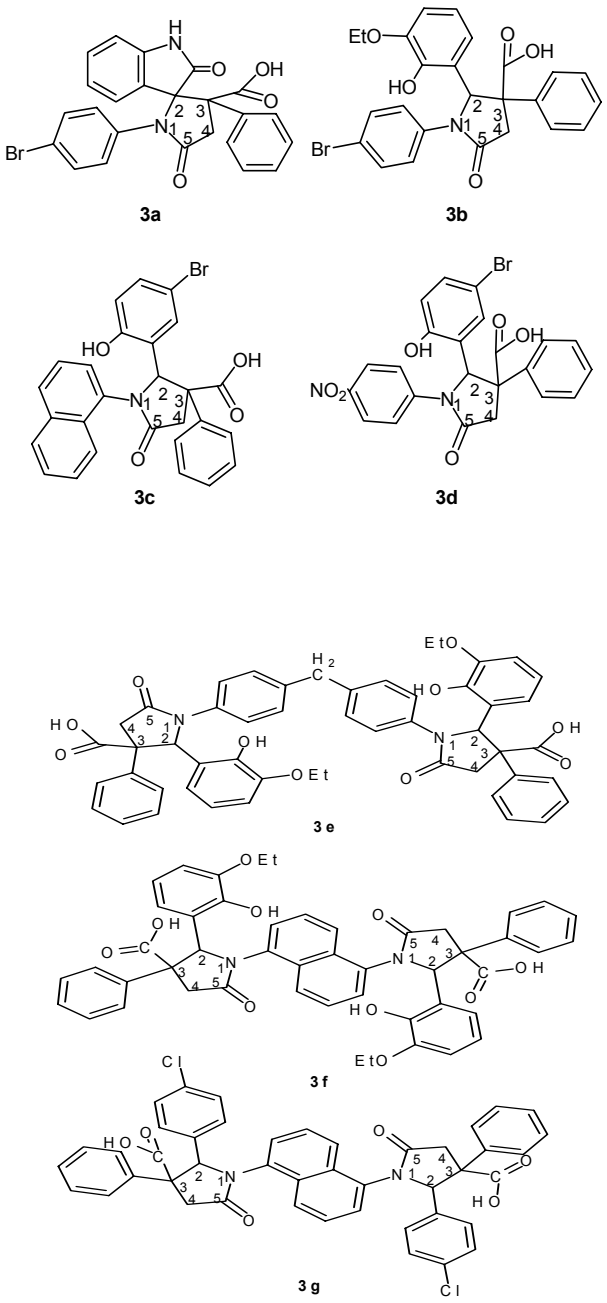

Figure 2. Structures of the compounds (**3a-3g**).

The compound was prepared by reacting 0.454 g (0.01mol) of **2f** with 0.352 g (0.02 mol) of phenylsuccinic anhydride. Yield 66 %, m.p. 146-147 ºC, colour orange. IR (KBr): 1636 cm^{-1} (HO-C=O), 1732 cm^{-1} (–N–C=O). ^{1}H-NMR (500 MHz, DMSO) δ = 1.86 (d, 6H, -CH_3), 3.7 (d, 4H, CH_2-O), 4.05 (d, 4H, C_4-H), 4.7 (d, 2H, -C_2-H), 7.4-8.5 (m, 24H, Ar-H), 9.5 (d, 2H, -OH), 10.7 (d, 2H, OHC=O).

1,1'-(Naphthalene-1,5-diyl)bis(2-(4-chlorophenyl)-5-oxo-3-phenylpyrrolidine-3-carboxylic acid) (3g)

The compound was prepared by reacting 0.6 g (0.01 mol) of **2g** with 0.525 g (0.02 mol) of phenylsuccinic anhydride. Yield 75 %, m.p. 190-193 ºC, colour greenish. IR (KBr): 1656 cm^{-1} (HO-C=O), 1706 cm^{-1} (–N–C=O). ^{1}H-NMR (500 MHz, DMSO) δ = 3.5 (d, 4H, C_4-H), 4.45 (d, 2H, -C_2-H), 7.6-8.3 (m, 24H, Ar-H), 11.0 (d, 2H, OHC=O).

Results and discussion

The structural skeleton of chiral lactams are found in a broad range of natural and biologically active molecules, such as penicillins, cephalosporins, carbapenems, monobactams, salinosporamide A, rolipram and brivaracetam.

In the present investigation, γ-lactams are obtained by the reaction of imines with phenylsuccinic anhydride to in a suitable solvent (dioxane or chloroform). The structures of the compounds **3a–3g**, as established by spectral analysis, are given in Fig. 2. A probable mechanism for synthesis has been suggested (Schemes 1 - 4).

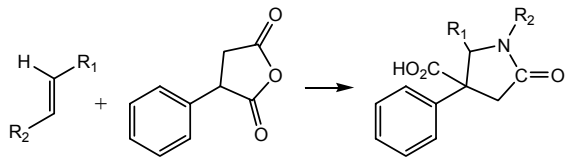

Scheme 1. Synthesis of mono γ-lactam

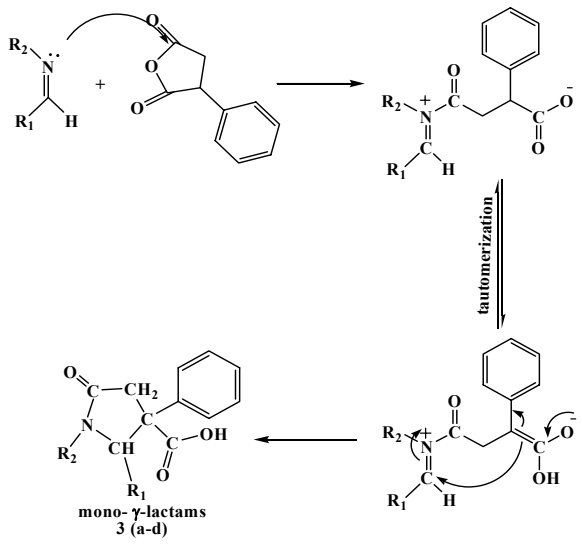

Scheme 2. Mechanism of formation of mono γ-lactam

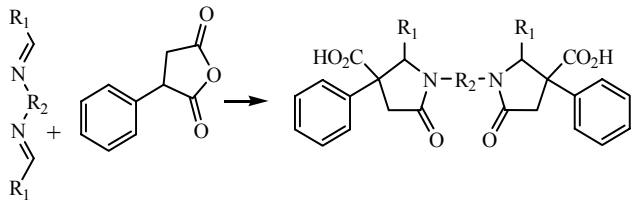

Scheme 3. Synthesis of bis γ-lactam

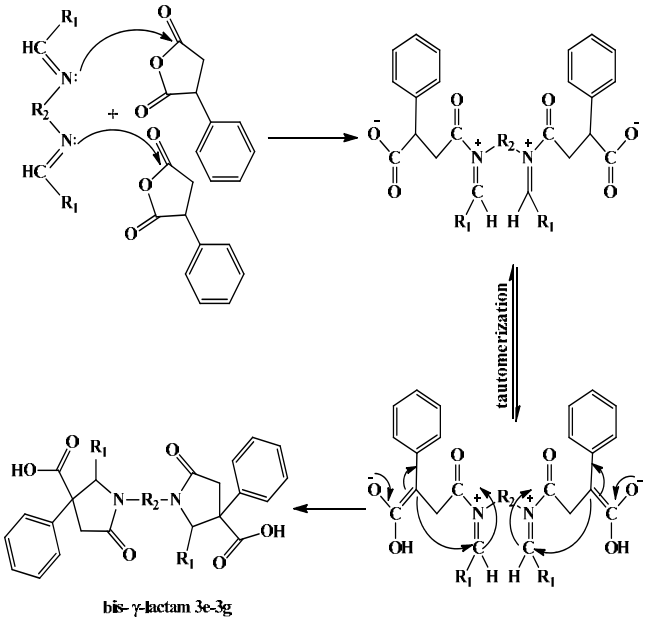

Scheme 4. Probable mechanism of the formation of bis-γ-lactams.

Analysis of infrared spectra

The IR spectra of mono and bis γ-lactams (**3a-3g)** are characterized by the seven bands corresponding to the stretching vibration of the aromatic C-H, aliphatic C-H, carbonyl carboxylic group, carbonyl amide group, aromatic C=C, C-N band and the substituted ring which occurs within the ranges 3126-3030, 2990- 2878, 1733-1706, 1699-1636, 1603-1568, 1340-1325, and 925-617 cm^{-1} respectively.

Analysis of ^{1}H-NMR spectra

The ^{1}H-NMR spectra (Figure 3) of **3a** showed γ-lactam ring singlet signal at δ = 3.3 ppm for methylene group (CH_2), multiplet signal at δ = 7.2 - 8.21 ppm for aromatic protons (m, 13H, Ar-H), singlet signal for one proton in γ-lactam ring at δ= 9.4 ppm for NH, and finally showed singlet signal for proton carboxylic acid at δ = 11.3 ppm.

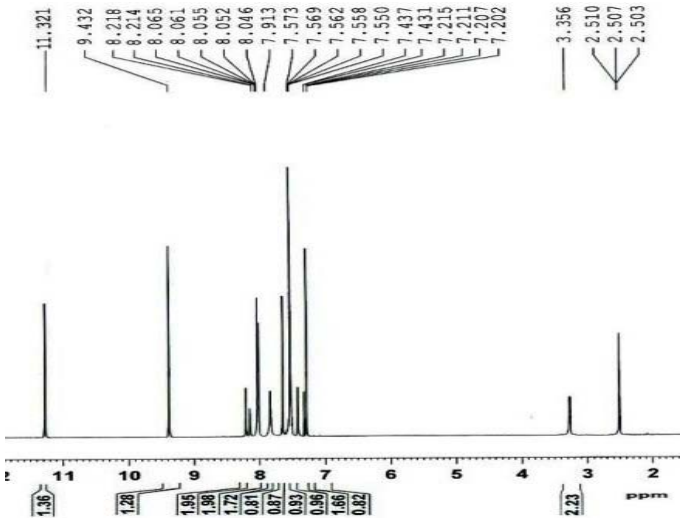

Figure 3. ^{1}H-NMR spectra of **3a**.

Analysis of ^{13}C-NMR spectra

The ^{13}C-NMR spectra (Figure 4) of **3a** showed in γ-lactam ring singlet signal at δ = 48 ppm for methylene group (C_4-H_2), at 52 ppm for C_2-ring, at 58 ppm for C_3-ring, at 174 ppm for O=C-ring, multiplet at 114-151 ppm for aromatic protons (m, C-Ar), at δ 175ppm for HN-C=O, and at 179 ppm for HO-C=O.

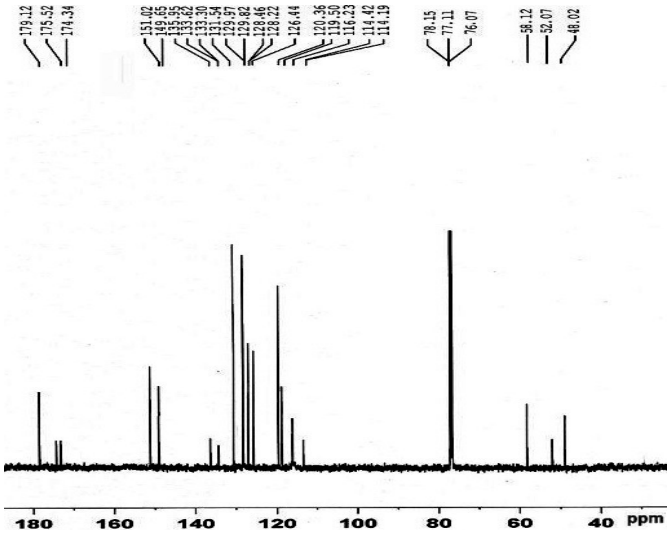

Figure 4. ^{13}C-NMR spectra of **3a**.

Analysis of mass spectra

The mass spectrum of **3a** shows the molecular ion peak corresponding to the particular compound at 477 m/z, and the fragmentation of **3a** showed the peaks at 346, 301, 198, 132, 104, 90 ,77,65 m/z which are attributed to the fragments of $C_{16}H_{12}BrNO_3^+$, $C_{15}H_{11}BrNO^+$, $C_7H_4BrNO^+$, $C_8H_6NO^+$, $C_7H_6N^+$, $C_7H_6^+$, $C_6H_5^+$ and $C_5H_5^+$ respectively.

The mass spectrum of **3b** shows the molecular ion peak corresponding to the compound at 496 m/z. The fragmentation of **3b** showed the peaks at 428, 467, 439, 422, 387, 329, 198, 131, 77 and 65 m/z which are attributed to the fragments of $C_{24}H_{20}BrNO_5^+$, $C_{23}H_{17}BrNO_5^+$, $C_{22}H_{17}BrNO_4^+$, $C_{22}H_{16}BrNO_3^+$, $C_{23}H_{17}NO_5^+$, $C_{16}H_{11}BrNO_2^+$, $C_7H_4BrNO^+$, $C_9H_7O^+$, $C_6H_5^+$, $C_5H_5^+$ respectively.

The mass spectrum of **3c** shows the molecular ion peak corresponding to the compound at 497 m/z. The fragmentation of **3c** showed the peaks at 312, 295, 267, 225, 174, 77 and 65 m/z which are attributed to the fragments of $C_{16}H_{12}N_2O_3^+$, $C_{16}H_{11}N_2O_4^+$, $C_{13}H_9N_2O_2^+$, $C_9H_9N_2O_2^+$, $C_6H_5^+$ and $C_5H_5^+$ respectively.

Analysis of ^{13}C-NMR DEPT spectra

^{13}C-NMR DEPT spectral of **3a** showed in γ-lactam ring singlet signal at δ = 48 (negative) ppm for methylene group (C_4-H_2), at 52 (positive) ppm for (C_2-ring), at 58 (positive) ppm for (C_3-ring), at 174 (positive) ppm for (O=C-ring) a multiplet signal at 116-151 (positive) ppm for aromatic protons (m, C-Ar), at 175 (positive) ppm for (HN-C=O) and a signal at 179 (positive) ppm for (HO-C=O).

^{13}C-NMR DEPTspectral of **3b** showed in γ-lactam ring singlet signal at δ = 42.11 (negative) ppm for methylene group (C_4-ring), at 49.17 (positive) ppm for C_2-ring, at 58.18 (positive) ppm for C_3-ring, at 173 (positive) ppm for O=C-ring, a multiplet at 115-158 (positive) ppm for aromatic protons (m, C-Ar), at 180 (positive) ppm for (HO-C=O), at 29 (positive) ppm for -CH_3 and a signal at 42 (negative) ppm for O-CH_2.

Acknowledgements

This work is sponsored by the university of Thi-Qar as a part of research development and higher studies projects.

References

[1]Catalani, M.., Alvaro, G., Bernasconi, G., Bettini, E., Bromidge, S. M., Heer, J., Tedesco, G., Tommasi, S., *Bioorg. Med. Chem. Lett.,* **2011,** *21,* 6899–6904.

[2]Lee, C., Choi, E., Cho, M., Lee, B., Oh, S. J., Park, S. K., Lee, K., Kim, H. M., Han, G., *Bioorg. Med. Chem. Lett.,* **2012,** *22,* 4189–4192.

[3]Cornut, D., Lemoine, H., Kanishchev, O., Okada, E., Albrieux, F., Beavogui, A. H., Bienvenu, A.-L., Picot, S., Bouillion, J.-P., Médebielle, M., *J. Med. Chem.,* **2013,** *56,* 73–83.

[4]Zhao, X., DiRocco, D. A., Rovis, T., *J. Am. Chem. Soc.,* **2011,** *133,*12466–12469.

[5]Comesse, S., Sanselme, M., Daïch, A., *J. Org. Chem.,* **2008,** *73,* 5566–5569.

[6]Zhang, Y., Shao, Y.-L., Xu, H.-S., Wang, W., *J. Org. Chem.,* **2011,** *76,* 1472–1474.

[7]Shao, C., Yu, H.-J., Wu, N.-Y., Tian, P., Wang, R., Feng, C.-G., Lin, G.-Q., *Org. Lett.,* **2011,** *13,* 788–791.

[8]Lin, L., Zhang, J., Ma, X., Fu, X., Wang, R., *Org. Lett.,* **2011,** *13,* 6410–6413.

[9]Hello, K. M., *Iraqi J. Chem*., **2000,** *24*, 266.

[10]Krishnaswamy, D., *Tetrahedron.*, **2002,** *34,* 4567.

[11]Abdulrhman, Y. K., Mahmood, S. M., *Best J.,* **2014,** *2(5)*, 37-48.

[12]Burdzhiev, N. T., Stanoeva, E. R., *Z. Naturforsch*., **2008,** *63b*, 313-320.

[13]Majeed, N. N., Esaa, A. H., Turki, A. A., *Pharm. Chem.,* **2014,** *6(2),* 288-293.

Received: 18.11.2016.
Accepted: 14.01.2017.

INFLUENCE OF THE SHAPE OF MAGNETIC PARTICLES AND DIELECTRIC PERMITTIVITY OF THE MEDIUM ON MAGNETO-OPTICAL PROPERTIES OF NANO-DISPERSIVE COBALT

Omar Nakashidze[a] and Lali Kalandadze[a]*

Keywords: Magneto-optical spectra, Effective medium approximation, Thin metal films.

The influence of the shape of magnetic particles and dielectric permittivity of the medium is investigated on the magneto-optical properties of the nano-dispersive structures using the thin discontinuous Co films. The behaviour of the magneto-optical spectra of thin Co films was explained in the framework of the effective medium approximation. The results have confirmed the significant change of the components of the tensor of effective dielectric permittivity and subsequently of the magneto-optical and optical properties which brought about the change of the shape of magnetic particles. These calculations proved that a good agreement between the experimental results and the theoretical calculations is achieved if the shape of the particles is taken into account

* Corresponding Author:
E-Mail: lali62@mail.ru
[a] Department of Physics, Batumi Shota Rustaveli State University, Batumi, Georgia

Introduction

The advance in technology requires magnetic materials with new properties. It is for this reason that intensive experimental and theoretical research on the magnetic substances is being pursued worldwide with a view to creating cutting-edge materials. The exploration of the mutual influence of the microstructure and the structural content on magnetic, magneto-optical and optical properties of nanoheterostructures has become the focus of intensive research. Therefore, experimental methods of magneto-optical researches are extremely relevant to study, as they allow the study of their inner electronic structures, and especially of their magnetic interactions. Optical and magneto-optical research methods are one of the simplest, the most effective and informative way of studying of the nanostructures and the modern materials.

Nowadays, magneto-optical research methods are widely used for examination of ultrafine magnetic structures such as: magnetic fluids, thin discontinuous metal films, heterogenic glasses, ferrite-garnet films, implanted magnetic surfaces, etc. Ultrafine medium is an ensemble of particles having smaller size than 100 nm. They have unique qualities compared to bulk ferromagnetic. This appears to be a result of the fact that the particles with identical properties and materials of particles are destroyed at a diapason covering size till 100 nm.[1,2]

There is no doubt that any experimental or theoretical research done in this direction revives a strong interest as many aspects still remain enigmatic.

Theory

In general, the magneto-optical properties of nano-dispersive magnetic structures are very different from the properties of the bulk ferromagnetic and depend on the structural parameters: the occupancy of the volume of the ultrafine medium with metal, the size and shape of the particles, the order of the particles, the properties of the medium, surrounding metal particles.[3,4]

The tensor of effective dielectric permittivity of magnetized ultrafine ferromagnetic material, by analogy with the tensor for bulk ferromagnetic materials, is represented as

$$\varepsilon_{eff} = \begin{bmatrix} \varepsilon_{eff} & -i\varepsilon'_{eff} & 0 \\ i\varepsilon'_{eff} & \varepsilon_{eff} & 0 \\ 0 & 0 & \varepsilon_{eff0} \end{bmatrix}, \quad (1)$$

where

$$\varepsilon_{eff} = \varepsilon_{1eff} - i\varepsilon_{2eff},$$
$$\varepsilon_{0eff} = \varepsilon_{01eff} - i\varepsilon_{02eff},$$
$$\varepsilon'_{eff} = \varepsilon'_{1eff} - i\varepsilon'_{2eff}.$$

In this case the tensor components depend on both the properties of magnetic colloidal particles themselves, and the properties of the medium in which they find themselves. The knowledge of tensor components enables us to calculate any type of magneto-optical effect. The next step is to establish the link between the components of the tensor of effective dielectric permittivity and the components of the tensor of the according bulk materials. This task was first brought in 1985.[5]

For ultrafine magnetic medium with a low concentration of magnetic colloidal particles and with no direct contact between them the tensor components of the effective dielectric permittivity within the framework of theoretical models of an effective medium, extended to include the case of magnetic media, can be written as:

1.The model of averaged characteristics:

$$\varepsilon_{eff} = q\varepsilon_m + (1-q)\varepsilon_0 ; \quad \varepsilon'_{eff} = q\varepsilon'_m \qquad (2)$$

2. The Maxwell–Garnett model:

$$\varepsilon_{eff} = \frac{2q(\varepsilon_m - \varepsilon_0) + (\varepsilon_m + 2\varepsilon_0)}{(\varepsilon_m + 2\varepsilon_0) - q(\varepsilon_m - \varepsilon_0)},$$

$$\varepsilon'_{eff} = \frac{9q\varepsilon_0^2\varepsilon'_m}{(\varepsilon_m(1-q) + \varepsilon_0(2+q))^2}. \qquad (3)$$

3. The Bruggeman model:

$$\varepsilon_{eff} = \varepsilon_o(1 + 3q\frac{\varepsilon_m - \varepsilon_o}{\varepsilon_m + 2\varepsilon_o}); \quad \varepsilon'_{eff} = \frac{9q\varepsilon_o^2\varepsilon'_m}{(\varepsilon_m + 2\varepsilon_O)^2}, \quad (4)$$

where

$\varepsilon_m=\varepsilon_{1m}-i\varepsilon_{2m}$ and $\varepsilon'_m=\varepsilon'_{1m}-i\varepsilon'_{2m}$, are the diagonal and nondiagonal tensor components of the dielectric permittivity of the material of magnetic colloidal particles,

ε_0 is the dielectric permittivity of the non-magnetic phase, and q is the ratio of the volume, occupied by magnetic particles, to the total volume of the magnetic fluid.

After generalization of this theory we arrive at a formula to calculate tensor components for non-spherical ultrafine particles:

$$\varepsilon_{eff} = \varepsilon_0\left(1 + \frac{q(\varepsilon_m - \varepsilon_0)}{y\varepsilon_m + (1-y)\varepsilon_0}\right),$$

$$\varepsilon'_{eff} = \frac{\varepsilon_0^2\varepsilon'_m}{\left[y\varepsilon_m + (1-y)\varepsilon_0\right]^2}, \qquad (5)$$

where

$y=f(1-q)$, whilst f is the factor of the shape of the ultrafine particles.[5]

These formulae (5) can be used to investigate which structural parameter has more influence on the optical and magneto-optical properties of the ultrafine medium.

The equatorial Kerr effect under consideration, which consists in a change in the intensity of linearly polarized light reflected from the sample in the case reversal of magnetization of the sample, can be written as

$$\delta_p = \frac{2\sin 2\varphi}{A^2 + B^2}\left(A\varepsilon'_{1eff} + B\varepsilon'_{2eff}\right), \qquad (6)$$

where

$A=\varepsilon_{2eff}(2\varepsilon_{1eff}f\cos^2\varphi-1)$

$B=(\varepsilon^2_{2eff}-e^2_{1eff}+1)\cos^2\varphi+e_{1eff}-1$

φ is the angle of light incidence.

Experimentals

The magneto-optical properties of discontinuous cobalt films, the weight thickness d (d=m/ρS), where m -film mass, ρ -metal density and S -film square) of which falls within the interval 1-30 nm is investigated. Discontinuous films were obtained by evaporation in vacuum of 10^{-5} Torr on glass substrates with a rate of 0.1 to 0.5 nm s^{-1}. The magneto-optical properties were measured at room temperature using the equatorial Kerr effect in the energy range 1.5 - 5.0 eV, the light incident angle being $\varphi=70^0$. The optical constants were determined using the Avery method.[6]

Results and Discussion

Fig. 1 presents the spectral dependences of the equatorial Kerr effect for the nano-dispersive cobalt with different weight thicknesses d and for polycrystalline cobalt.

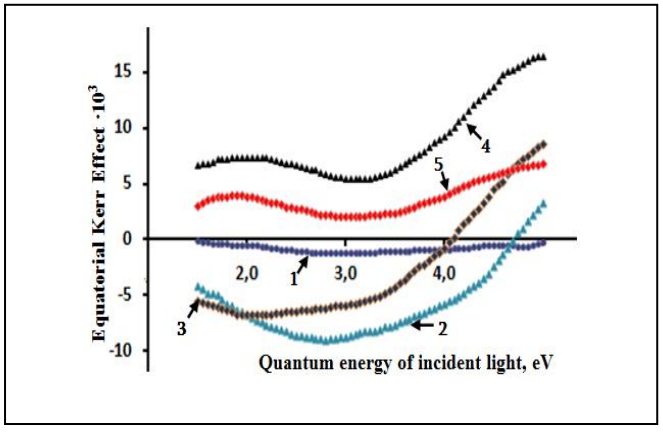

Figure 1. Experimental dependences of the equatorial Kerr effect on $\hbar\omega$ for Co films with weight thicknesses d=1.2 (1); 2.3 (2); 4.9 (3); 30 nm (4) and for polycrystalline Co films (5); (φ=70°).

It can be seen from the Figure 1 that for the films with different weight thickness the frequency dependences of the equatorial Kerr effect is significantly different from that of the similar dependences for bulk cobalt and depends on the film's effective thickness.

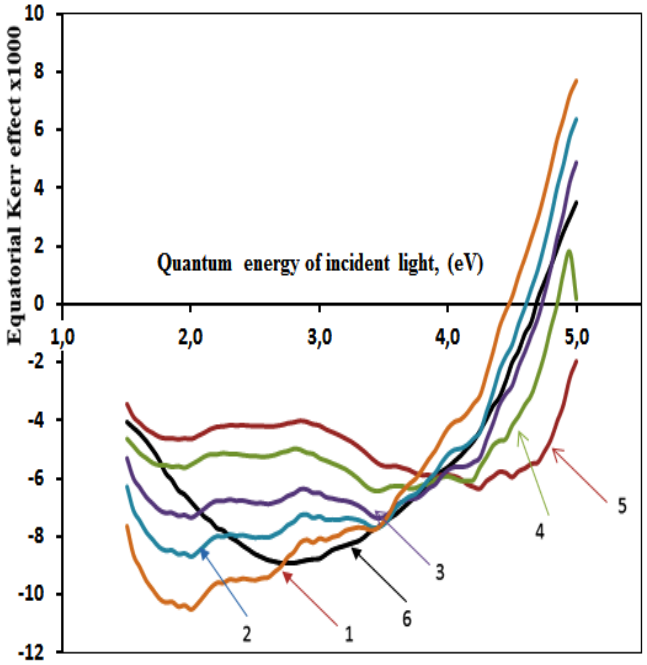

Figure 2. The calculated equatorial Kerr effect spectra of the nano-dispersive cobalt for q=0.2, f=1/3 and for different e_0=2.0 (Curve 1), 1.8 (Curve 2), 1.6 (Curve 3), 1.3 (Curve 4), 1.0 (Curve 5) and experimental dependences for Co films with 1.2 nm (Curve 6).

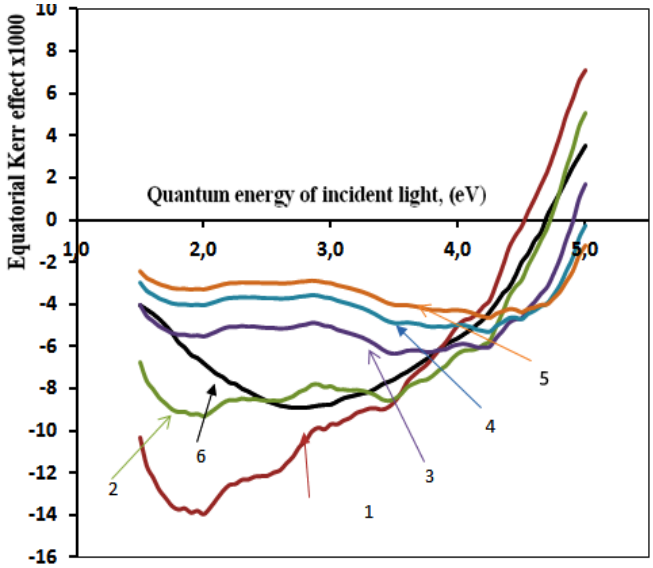

Figure 3. The calculated equatorial Kerr effect spectra of the nano-dispersive cobalt for q=0.2, ε_0=1.3 and for different f=0.2 (Curve 1), 0.25 (Curve 2), 1/3 (Curve 3), 0.4 (Curve 4), 0.45 (Curve 5) and experimental dependences for Co films with 1.2 nm (Curve 6).

The experimental results were compared with calculations in the framework of the effective medium approximation Eqn. (5) that allows to make some conclusions about dielectric permittivity of the medium and shape of magnetic particles. Fig. 2 gives the dependences of equatorial Kerr effect on the quantum energy of incident light, $\hbar\omega$, calculated by Eqns. (5) and (6) for namo-dispersive cobalt for different ε_0, and q=0.2, f=1/3. In this and following calculations the dielectric permittivity tensor components for bulk cobalt were used.

In Fig. 3 the frequency dependences of equatorial Kerr effect are presented for nano-dispersive cobalt with different values of the shape factor f, calculated in the framework of the effective medium approximation Eqn. (5) for q=0.2. In our case ε_0=1.3.

It is evident from the Figure 3 that the shape of magnetic particles influence significantly the magneto-optical properties of nano-dispersive cobalt.

Conclusion

The influence of the shape of magnetic particles and dielectric permittivity of the medium on the magneto-optical properties of the ultrafine metal films is investigated using the nano-dispersive cobalt as examples. The results have confirmed the significant change of the components of the tensor of effective dielectric permittivity and subsequently of the magneto-optical and optical properties which was brought about by the change of the shape of magnetic particles.

These calculations proved that if we take into account the shape of the particles, we will achieve a good agreement of the experimental results and the theoretical calculations.

Acknowledgement

This paper has been presented at the 4th International Conference "Nanotechnologies", October 24 – 27, 2016, Tbilisi, Georgia (Nano – 2016).

References

[1]1Lisserger, P. H, Saunders, P. W., *Thin Solid Films*, **1976,** *34*, 323-333.

[2]Kalandadze, L., *J. Sensor Lett.*, **2007**, *5(1)*, 13-14.

[3]Nakashidze, O. and Kalandadze, L., *Influence of Shape of Magnetic Particles on Magneto-Optical Properties of the Ultrafine Structures. New Developments in Materials Science*; Nova Publishers; **2013,** 119-126

[4]Gan'shina, E., Granovsky, A., Guschin, V., Perov, N., Dieny, B., *Magnetism Magn. Mater.*, **1997**, *165*, 320-322

[5]Nikitin, L V. and Kasatkina, O. V., *Proc. X All-Union School-semin. New Magnetic Mater. Microelectronics (Riga)* **1986**, *2*, 124 (in Russian).

[6]Avery, D. G., *Proc. Phys, Soc.*, **1952**, *65B*, 426.

Received: 27.11.2016.
Accepted: 14.01.2017.

1,2-HYDROGEN MIGRATION IN AMINOALKYL RADICALS IN AMINATION REACTIONS OF α-OLEPHINS

T. A. Aslanov,[a] E. T. Aslanova,[a]* N. R. Bektashi,[a] A. H. Azizov[a] and D. R. Nurullayeva[a]

Keywords: α-olefins, 1,2-hydrogen migration, diamines, telomers.

The amination of α-olefins (C_4-C_7) in the NH_2OH·HCl-$TiCl_3$ oxidation-reduction system was investigated and a number of mono- and diamines were prepared. It has been found that in the attack of NH_2-radical to olefin a hydrogen migration from first carbon to second one takes place. It has been shown that in the reaction products, besides the desired individual amines, telomers, the molecular masses of which are approximately within the ranges of M_n = 460-800, were also detected.

* Corresponding Authors
Fax: (+99418) 642-04-00
E-Mail: ipoma@science.az
[a] Institute of Polymer Materials, Azerbaijan National Academy of Sciences, 124, S.Vurgun str., Az5004, Sumgait, Azerbaijan

Introduction

A study of the molecular rearrangements has a great value for establishment of mechanisms of the chemical reactions and realization of the directed organic synthesis. As it was known, the rearrangements are the reactions, in the course of which a substituent is displaced inside of the molecule from one place to another, breaking an old bond and creating a new.[1] There are 2 types of the rearrangements, rearrangements with reconstruction of carbon skeleton and rearrangements with conservation of carbon skeleton.

There are many rearrangements in the course of which a substituent from the carbon atom is transferred to the neighboring carbon, nitrogen or oxygen atoms. The similar 1,2-displacements can be caused by availability of electrons sextet (nucleophilic rearrangement), free electron pair of atom B (electrophilic rearrangement) or unpaired electron (radical rearrangement).

It has been reported earlier that in a number of the chemical reactions successive rearrangements take place.[2] Such reactions cause a lot of difficulties in establishment of the structure of the products.

It has been held earlier that, in solutions, the rearrangements of radicals are impossible or such processes are rare. So, Dewar[3] has explained the impossibility of isomerization of fatty radicals stating that in this case the stable π-complexes cannot be formed. Moreover, the absence of the rearrangement in neopentyl residue in action of sodium on neopentyl chloride has been cited as a proof of radical mechanism of Wurtz reaction.[4]

The first homolytic rearrangement proceeding in liquid phase was reported by Kharash in 1944, rearrangement of neophilic (2-phenyl-2,2-dimethylethyl) radical to a tertiary radical. Freidlina with collaborators (1950-1965) have systematically investigated the homolytic rearrangements of the aliphatic unsaturated haloid substituted compounds, rearrangements of allyl type.[5,6] Nesmeyanov with collaborators[5] have studied the isomerization of the radicals with 1,2-chlorine transfer. During study of pinacolone rearrangement occurring by the action of acids, particularly Lewis acids on pinacoles, Tiffen, Orekhov and Bakhman have studied in detail the ease of migration of radicals in this rearrangement.[7] The order of ease of migration the radicals has been reported as the following series:

$$n\text{-}CH_3OC_6H_4 > n\text{-}CH_3C_6H_4 > C_6H_5 > n\text{-}ClC_6H_4 > \text{Alkyls} > H$$

Reviews devoted to the rearrangements of radicals in the liquid phase are extremely rare. We could find only a small review published in Japan language,[8] and a brief summary about some questions of the rearrangement of radicals in solutions.[9,10]

This work is devoted to reactions of NH_2-radicals with α-olefins. It was known that NH_2-radicals take one of the central places in the chemistry of free radicals because they are the founder of an extensive series of nitrogen-centered radicals important for organic synthesis. At the same time, their reactions with organic compounds have not been investigated enough. There are few reports available in the literature that NH_2-radicals can be added to 1,3-dienes. On the basis of this reaction the synthesis of unsaturated diamines has been carried out. The reaction of NH_2-radicals with the simplest α-olefins has not been investigated until now, although it opens the most rational way of transition from unsaturated hydrocarbons to aliphatic amines.

In connection with above-mentioned one, the purpose of our work is the investigation of reaction of free-radical amination of α-olefins of composition C_4-C_7 in the oxidation-reduction system of NH_2OH·HCl-$TiCl_3$.

Experimental

The amination of α-olefins was carried out on basis of reported methodology.[11]

The ^{1}H-NMR-spectra were taken on a T-80 Varian spectrometer with working frequency 80 MHz, solvent was CCl_4 with hexamethyldisiloxane (HNDSO) as an internal standard. The chemical shifts (δ ppm) were measured in a scale with exactness 0.01 ppm. The IR-spectra were taken on a Specord M-80 apparatus in the vaseline oil.

The chromatographic investigations were carried out by the methods of gas-liquid, exclusion and adsorption liquid chromatography (GLC, ELC and ALC). The analysis of amines by a method of GLC was carried out on a Khrom-31 apparatus, gas-bearer was helium, column temperature 130-140 °C, column length 2.4 m, d = 4 mm, Chromaton + 1 % Carbowax served as a hard phase. The investigations by the methods of ELC and ALC were carried out on the high-effective liquid chromatograph of Czech firm, Kovo, with two columns by the size of 3.3×150 mm, filled with Separon SGX adsorbents, with diameter of pores 100 Å and Separon SGXC18 in the reversed phase respectively, particle size being 7 μm. There were chosen two-detector variants of these methods with use of UV-spectrophotometric (λ = 254 nm) and refractometric detectors. Eluents: dimethylformamide and methanol + water (75:25 rev.%). Their feed rate was 0.3 mL min^{-1}, temperature = 20-25 °C.

The molecular weights (MW) of amination products have been established on calibration dependence between log M and V_R prepared in ALC regime with application of mono- and diaminohexene and polyethylene glycol standards,[12] and also with use of the universal calibration dependence presented in an earlier work.[13]

Results and Discussion

Structure of amination reaction products of 1-butene

For synthesis of amino compounds on the basis of free-radical amination of α-olefins, generation of amine radical by the oxidation-reduction system $NH_2OH{\cdot}HCl$-$TiCl_3$ has been used. According to the previous reports of this reaction,[14,15] a formation of $\dot{N}H_2$ is presented as:

$$NH_2OH{\cdot}HCl + TiCl_3 \leftrightarrows \dot{N}H_2 + H_2O + TiCl_4 \quad (1)$$

For the generation of NH_2 radical, the oxidation-reduction system described earlier[14,15] has been chosen with only difference that instead of $TiCl_3$ taken in equimolar amount to hydroxylamine, a much smaller amounts of $TiCl_4$ has been taken, which reduced in $TiCl_3$ by hydrogen, generated in situ with Zn/HCI. During amination of α-olefins, as a result of their reaction with NH_2-radical, an aminoalkyl free radical is formed, the low selectivity of which leads to the formation of various products. An amination of 1-butene occurs on the following scheme

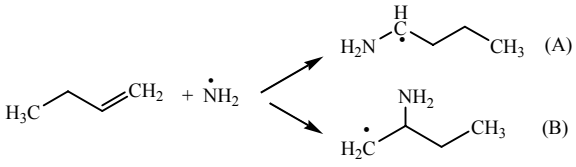

Scheme 1. Amination of 1-butene

Because of the high reactivity of radicals (A) and (B), a mixture of various amino compounds has resulted on the amination of 1-butene. During distillation of the reaction products two fractions with wide range of boiling temperature of 60-90 °C and 50-78 °C (5 mmHg) were obtained. The analysis of both fractions by a method of gas-liquid chromatography showed that the first of them is the mixture of monoamine of composition C_4,[11] and the second fraction is a mixture of primary and secondary diamines.

MW of the first fraction determined by cryoscopic method is 73.00, corresponding to a monoamine. From multiple experiments by precise purification of one fraction at boiling temperature 76-78 °C on column the isomer (98.8 %) corresponding to the second peak on chromatogram has been isolated. The calculated and found molecular rectification corresponded to butylamine ($MR_{D\ calc}$ = 27.30; $MR_{D\ found}$ = 26.90). The IR- and PMR-spectra of this substance were taken. In the IR-spectrum the characteristic absorption bands of aminogroup (valence vibrations) ν_{as} and ν_s at 3300 and 3370 cm^{-1}, deformation vibrations δ_s 840, 1400-1440 cm^{-1}, CH_2-groups ν_s 2850 cm^{-1}, δ_s 1470 cm^{-1}, CH_3-groups ν_{as} 2960 cm^{-1}, ν_s 2970 cm^{-1} have been observed. In the ^{1}H-NMR-spectrum, the characteristic chemical shifts in the field of δ=1.05, 1.3, 1.75 and 3.5 ppm, corresponding to protons in the groups NH_2, CH_3, CH_2-C and CH_2-N, with relation of the integral intensities 4:6:8:4, which confirms it to be butylamine.

The IR- and ^{1}H-NMR spectra of monoamine fraction boiling between 60 and 90 °C indicated to presence of 2-aminobutane in considerable quantity in it, supported by a 18 % chromatographic peak of this compound. Consequently, an activation of 1-butene in the present reaction takes place mainly in position 2, and only a small amount of butylamine is formed as a result of the attack of olefin molecule by NH_2-radical to position 1.

During chromatography of the fraction, boiling between 50 and 78 °C (5 mmHg.), after repeated precise rectification on two different sorbents, three peaks appeared in the chromatgram. The molecular refraction found and calculated for proposed structures of formed diamino compounds corresponded to $MR_{Dcalc.}$ = 46.05 and $MR_{D\ found.}$ = 45.78. In the IR-spectra of this fraction, the characteristic absorption bands of aminogroup ν_s, ν_{as} at 3370, 3300, 1640 cm^{-1}, CH_2-group at ν_{as}- 2850 cm^{-1}, CH_3-group at δ_{as} 2960, δ 1460 cm^{-1}, and for CH-group at δ 1340 cm^{-1} have been observed.

By precise rectification on vacuum column, the isomer corresponding to third peak on the chromatogram has been isolated. In the ^{1}H-NMR spectrum of this fraction, a number of groups of signals in the field of high areas were observed. In the range of 0.7-1.4 ppm there appeared two superimposed signals with unresolved multiplets. Besides, the signal with center at 0.85 ppm corresponded to the ten protons of fragment -CH_2-CH_3 on chemical shift and integral intensity, and other one with center at 1.2 ppm showed the superimposed signals of two methylene groups located in β-position to nitrogen atom. Four protons with δ = 1.63 ppm corresponding to protons of two amine groups $(NH_2)_2$. On dilution, the signal from amine protons displaced to the field of strong areas (δ = 1.02 ppm), which also witnessed an enhancement of sharpness of amino group signals. It may be noted that protons of amino groups participate in chemical exchange and therefore their

chemical shift unlike other signals is displaced with change of concentration. The signal at δ = 2.5 ppm on integral intensity corresponded to two protons. This signal should be attributed to methine protons at the nitrogen, a chemical shift of which is well consistent with the literary data.[16-19]

The assignment of integral intensities of protons of groups CH : NH_2 : -CH_2-CH_2-CH_3 equal to 8 : 15 : 56, exactly corresponding to the structure of 4,5-diaminooctane.

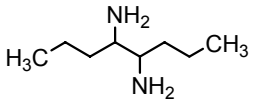

As the attack of NH_2-radical on C_1 is predominating, the formation of 4,5-diaminooctane can be explained by assuming migration of a hydrogen from C_1 to C_2 and dimerization of the resultant aminoalkyl radical.

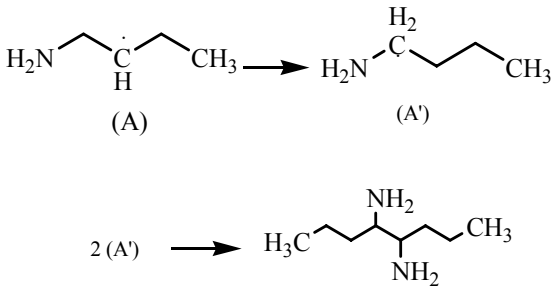

Scheme 2. Probable mechanism of the formation of 4,5-diaminooctane.

Structure of amination reaction products of 1-pentene

During amination of 1-pentene, the basic reaction products were mono-(C_5) and diamines (C_{10}) of isomeric composition. During vacuum distillation of the reaction product two fractions with boiling temperature, 95-106 °C and 90-100 °C (6 mmHg) have been isolated.

The chromatography of fraction boiling at temperature 95-106 °C indicated the presence of two peaks corresponding to two isomeric amylamine in it. MW fractions determined cryoscopically showed the satisfactory correspondence between their measured and theoretically calculated values (87.10). This fraction was subjected to the repeated precise fractionation as a result of a fraction boiling at 104 °C has been isolated. Chromatography of this fraction on the two different sorbents indicated that it is an individual substance. The observed MR_D of this substance is 25.80, and calculated for 1-aminopentene is 26.20. In the IR-spectrum of this compounds the characteristic absorption bands of amino group i.e. valence vibrations ν_{as} and ν_s = 3300 and 3370 cm^{-1}, deformation vibrations ν_{as}, ν_s - 840, 1400-1440 cm^{-1}, of CH_2-group ν_s 2850 cm^{-1}, δ_s 1470 cm^{-1} and of CH_3-group ν_{as} 2960 cm^{-1}, ν_s 2970 cm^{-1} were observed. In the ^{1}H-NMR spectrum there were the characteristic chemical shifts at 1.05, 1.75, 3.5 ppm corresponding to protons in NH_2, CH_3, CH_2-C, CH_2-N groups with relation of the integral intensities of 2:2:9, which confirmed the formation of 1-aminopentene.

In the IR-spectrum of the fractions with boiling temperature = 90-100 °C (6 mmHg), the characteristic absorption bands of amino group, ν_s and ν_{as}=3370 and 3300 cm^{-1}, δ 1640 cm^{-1}, of CH_2-group ν_{as} 2850 cm^{-1}, of CH_3-group ν_{as} 2960 and δ 1460 cm^{-1}, and of CH-group δ 1340 cm^{-1} were observed.

In the ^{1}H-NMR spectrum, in the region of high fields in the range of 0.7-1.4 two partially superimposed signals with unresolved multiplets were observed. The signal with center at 0.85 ppm and integral intensity of ten protons of the fragment corresponded to -CH_2, -CH_3, and other one with center at 1.20 ppm are the superposed signals of protons of two methylene groups located in β-position to nitrogen atom. The signals of four protons with δ = 1.63 ppm corresponded to the amines displaced to strong fields (δ = 1.02 ppm), with also witnessed the sharpness assignment of the amino group. The moderate signal at δ = 2.5 ppm with integral intensity corresponding to two methylene protons is in agreement with literary data. The assignment of the integral intensities of protons in groups CH_3 : NH_2 : -CH_2-CH_2-CH_3 = 8 : 15 : 70 (calculation = 2 : 4 : 18) confirms the formation of 5,6-diaminodecane.

The results of the experiment indicated that with an increase in the molecular weight of the olefin the relative amount of diamine formed, as a result of dimerization of the initially formed aminoalkyl radicals, is decreased.

The results of establishment of structure of the amination reaction products of α-pentene by physicochemical methods of analysis showed that they are 1-aminopentane (I), 2-aminopentane (II), 5,6-diaminodecane (III), 4,7-diaminodecane (IV) and 4,6-diaminodecane (V). The formation of which has been presented in Scheme 3.

Structure of products of amination of 1-hexene

As a result of amination reaction of 1-hexene, two fractions with boiling temperature 132-133 °C and 120-130 °C (2 mmHg) have been isolated.

In the IR-spectrum of the first fraction the intensive absorption bands of valence vibrations of NH_2-group at 3386 and 3300 cm^{-1}, correspondingly to asymmetric (ν_{as}) and symmetric (ν_s) vibrations were observed. A calculation of ν_s on formula ν_s = 345.5 + 0.876, ν_{as} = 345.5+ 0.876· 3386 = 3302 cm^{-1} is sufficiently well agreed with observing in 3300 cm^{-1}. The deformation vibrations of amino group were observed by the broadened bands in the range of 840 and 1600 cm^{-1}. The presence of CH_2-groups is confirmed by absorption bands in the range of 2920 cm^{-1} and 1460 cm^{-1}.

In the NMR-spectrum of this fraction the characteristic singlet at δ = 0.95 ppm, corresponding to two protons of NH_2-group was observed. The broadened (due to influence of nitrogen atom) signal at δ = 2.6 ppm on integral intensity corresponded to two protons of CH_2-group. The chemical shift of these protons located at nitrogen atom is in accordance with the reported values. Triplet δ = 1 ppm corresponded to methyl protons. The signals in the field of 1.15-1.25 ppm showed the presence of protons in methylene group connected to a carbon atom i.e. a -CH_2-C group.

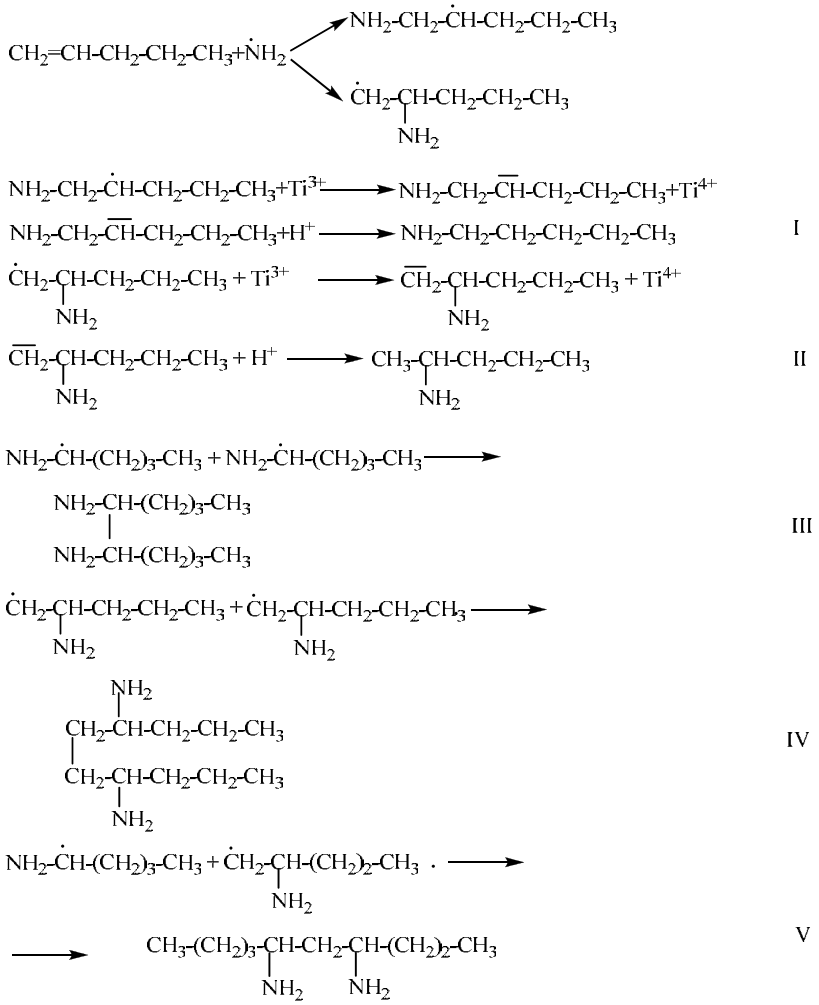

Scheme 3. Probable mechanism of the formation of products by the amination of 1-pentene.

Thus, in the spectrum there were the signals of the following groups: CH_3 : -CH_2-C : CH_2-N : NH_2 with ratio of integral intensities = 8:24:6:5, which are close to calculated quantity of protons in hexylamine, 3:8:2:2.

The investigation of fraction boiling at 120-130 °C (2 mmHg) by GLC showed the availability of two compounds in the ratio of 8:1. By precise fractionation of the fraction, a product present in the mixture in 87.6 % has been isolated. In the IR-spectrum of this product the absorption bands of amino group (ν_s, ν_{as} = 3370 and 3300 cm^{-1}, δ = 1640 cm^{-1}), CH_2-group (ν_s = 2850 cm^{-1}), CH_3-group (ν = 2960, δ = 1460 cm^{-1}) and CH-group (δ = 1340 cm^{-1}) were observed. In the ^{1}H-NMR-spectrum of the same product there was a triplet with center at δ = 0.85 ppm for 6 H corresponding to two methyl groups. The signal at δ = 1.2 was assigned to the superimposed signals of methylene protons, methine groups and finally the signal at δ = 1.2 met the superimposed signals of methylene protons located in β-position to nitrogen atom. Four protons at δ = 1.8 corresponded to $(NH_2)_2$ amine protons. on dilution, the signal from amine protons was displaced to strong fields (δ = 1.25 ppm), which supported their assignment to amino protons. The signal δ = 2.45 corresponded to methine protons at nitrogen. Thus, in the spectrum there were observed the signals of groups: CH_3: -CH_2-C : CH_2-N : NH_2 with relation of integral intensities equal to 15:40:4:9, which is close to calculated quantity of protons (6:16:2:4) in molecule of diaminododecane.

Thus, on the basis of ^{1}H-NMR-spectrum the compound can be assigned the following formula.

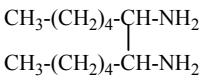

The investigations showed with an increase in molecular weight of the aminated α-olefin, the addition of NH_2-radical to the second carbon atom is considerably decreased. As a result in addition to diamine, formed from dimerization of type (A) radical, high molecular weight telomeric products are also formed.

Structure of products of amination of 1-heptene

As a result of distillation of the amination products of heptene-1, two fractions have been isolated, with boiling at 158 °C and 135-140 °C (2 mmHg).

The chromatographic analysis showed the first fraction to be an individual compound. In the IR-spectrum of this compound, the characteristic absorption bands at 3295 cm^{-1} and 3380 cm^{-1} (ν_s, ν_{as}), and also at 1600 and 840 cm^{-1} (deformation), corresponding to vibrations of amino group, at 2890 and 1340 cm^{-1} for CH_2-groups and 2975 cm^{-1} for CH_3- groups have been observed. In the ^{1}H-NMR-spectrum of this compound the signals corresponding to these groups are also observed. Triplet at δ = 0.95 ppm corresponds to the protons of end methyl group and the superimposed signals of methylene groups, not connected with nitrogen atom, appear at δ = 1.3 ppm. The signal at δ = 2.5-2.8 ppm corresponds to the protons of -CH_2-N and NH_2-groups. The signals of NH_2-groups appeared as a sharp singlet within the multiplet signals of CH_2-N. The integral intensity of the signals of CH_3 : CH_2-C : CH_2-N : NH_2 = 17 : 50 : 20 corresponding to the calculated quantity of protons in heptyl amine i.e. 3:10:4.

In the ^{1}H-NMR-spectrum of the fraction, boiling at 135-140 °C (2 mmHg), the signals were analogous to those of 6,7- diaminododecane with only difference that the quantity of protons in hydrocarbon residue has increased. The ratio of integral intensities of the signals in the -spectrum of CH_3 : CH_2 : CH_2 : -N : NH_2 = 21 : 68 : 16 : 8 corresponded to the calculated value of 3 : 10 : 1 : 2, which also confirmed the formation of 7,8-diaminotetradecane during amination of 1-heptene.

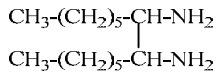

Mechanism of formation of telomers during amination of 1-hexene

The mechanism of the amination process of α-olefins and formation of high-molecular telomers therein has been investigated in the case 1-hexene. The analysis involved ALC on reversed phase and ELC with two-detector system of chromatography.[20] As a result of analyses of the reaction products by refractometric detection, 5 fractions have been detected, 3 of which correspond to the high-molecular telomers in a quantity of 5, 14 and 6 % with molecular weight M_n = 794, 660 and 478, respectively. Two subsequent fractions consist of monoamine (70 %) and from mixture of isomers of diamino compounds, i.e. 6,7- and 5,8-diaminododecane (5 %). These compounds are the dimerization products of aminoalkyl radicals forming in attack of NH_2-radical to molecule of 1-hexene, which leads to the proton transfer from first carbon atom to the second and vice versa from second to the first one. It has been established that the hydrogen migration also influences the isomeric structure of telomers products. So, unlike refractometer readings the signals of telomere fractions on the working wave (254 nm) of UV-detector have a multiplet character and consist of three maxima, which can be referred to various isomers of oligoaminohexene, most likely formed during proton migration between different carbon atoms.

Conclusions

1. It has been shown that the synthesis of amino compounds of C_4-C_7 α-olefins by the oxidation-reduction system $NH_2OH{\cdot}HCl$-$TiCl_3$ takes place by an attack of NH_2-radical predominantly on first and to a lesser extent on second carbon atom, accompanied by hydrogen migration from C_1 to the C_2 (1,2-migration) and vice-versa (2,1-migration), leading to the formation of α- and β-monoaminoalkanes. A dimerization of arising aminoalkyl radicals leads to the formation of the higher diaminoalkanes.

2. It has been established that in the case of amination of 1-hexene and 1-heptene, along with the formation of individual aminoalkanes, telomerization of the corresponding olefins leading to appearance of fractions of oligomer amines with MW 500-800 (in the case of 1-hexene) and 700-950 (in the case of 1-heptene) takes place.

3. It has been established by a method of reversed-phase ALC in example hexene-1 that each telomer fraction consists of mixture of three isomers. So, on the working wave length of UV-spectroscopic detector (λ = 254 nm) the triplet signals corresponding to the different isomers of oligoaminohexene with the same MW have been fixed. It has been concluded in accordance with regularities of reversed-phase ALC that the separation of these isomers occurs in the order of decreasing of their polarity. The accordance of the first two isomers to more polar α- and β-oligoaminohexanes forming at 1,2- and 2,1-hydrogen migration and third, less polar isomer corresponding to oligohexane forming by hydrogen migration either from second to the third, or to the fourth carbon atom has been shown.

References

[1]Grin, M. A., Mironov, A. F., *Rearrangements in thin organic synthesis*, Moscow, **2005**.

[2]Freydlina, R. Kh., Kost, V. N., Khorlina, M. Ya., *Usp. Khim.*, **1962**, 31*(1)*, 3.

[3]Dewar, M. J. S., *The Electronic Theory of organic chemistry,* Oxford, **1949**.

[4]Dupon, G., Dulon, R., Clement, G., *Bull. Soc. Chim. Fr.*, **1950**, *1056*, 1115.

[5]Nesmeyanov, A. N., Freidlina, R. Kh., Zakharkin, L. N., *Dokl. AN SSSR*, **1951**, *81(2)*, 199.

[6]Freidlina, R. Kh., *Adv. Free Radical Chem.*, **1965**, *1*, 211.

[7]Nesmeyanov, A. N., Nesmeyanov, N. A., *Nachala organicheskoy khimii*, *Khimiya*, **1974**, *II,* 744.

[8]Okawa, M., *Kagaku(Kyoto),* **1955**, *10(1)*, 39.

[9]Walling, Ch., *Free Radicals in solution, Wiley, New York*, **1957**.

[10]Nesmeyanov, N. N., *O nekotoryh problemah khimicheskoy kinetiki i reakcionnoy sposobnosti*, *AN SSSR*, **1958**.

[11]Aslanov, T. A., Mustafayev, R. I., *Neftekhimiya*, **1988**, *27(4)*, 541-542.

[12]Bektashi, N. R., Aliyeva, D. N., Dzhalilov, R. A. and Ragimov, A. V., *Polym. Sci.,* **2000 B**, *42(10-11),* 1769-1774.

[13]Bektashi, N. R., Mustafayev, A. M., Guseinov, I. A., Mustafayev, S. G., Dzhafarov, V. D., *Russ. J. Appl. Chem.*, **2011**, *84(7)*, 1281-1287.

[14]Davis, P., Evans, M. G., Higginson, W. C., *J. Chem. Soc.*, **1951**, 2563-2567.

[15]Albiseti, C. J., Coffman, D. R., Hoover, F. W., Jenner, E. Z., Mochel, W. E., *J. Am. Chem. Soc.*, **1959**, *81(6)*, 1489-1494.

[16]Ionin, B. I., Ershov, B. A., *NMR-spectroscopy in organic chemistry*, Khimiya (Russia), **1967**.

[17]Zhunke, A., *NMR-spectroscopy in organic chemistry*, Mir, Russia, **1974**.

[18]Gadzhiyev, T. A., Mustafayev, A. M., Aslanov, T. A., *SU 507560*.

[19]Gadzhiyev, T. A., Aslanov, T. A., Mkrtycheva, E. M., *Plast. Massy*, **1977**, *5*, 75.

[20]Bektashi, N. R., *25 Uluslararası katılımlı Ulusal kimya kongresi, Turkiye, Erzurum, 28 haziran 2 temmuz*, **2011**, *P.188*, 207.

Received: 14.11.2016.
Accepted: 14.01.2017.